[redacted]

DIAGNOSTICS AND INTERPRETATION OF ACCELERATION MECHANISMS IN AN MPD ARC

D. R. Brooks, J. M. Hoell, Jr., R. V. Hess,
and P. Brockman

NASA Langley Research Center
Langley Station, Hampton, Va.

Presented at the AIAA Joint Electric Propulsion
and Plasmadynamics Conference

Colorado Springs, Colorado
September 11-13, 1967

DIAGNOSTICS AND INTERPRETATION OF ACCELERATION MECHANISMS IN AN MPD ARC

D. R. Brooks, J. M. Hoell, Jr., R. V. Hess,
and P. Brockman
NASA Langley Research Center
Langley Station, Hampton, Va.

Abstract

Experimental results are presented for distributions of current, potential, electron density, electron pressure, and ion velocity vector orientation in a hollow-cathode porous-anode MPD arc. The presence of electromagnetic effects is verified by the existence of large radial electric fields and axial currents extending several anode diameters downstream from the electrodes. Additional evidence is provided by observation of the conversion of ion rotational velocity into translation (although the magnitude of the velocities has not been established). A relatively large azimuthal current of unknown magnitude and distribution has been found. It is shown that electrothermal fields ($\nabla P_e/ne$) can be as large as electric fields in some regions of the arc exhaust. Despite a large number of simplifications made in analysis, numerical solutions to Laplace's equation have yielded potential surveys which agree qualitatively with experiment. Examples of computed equipotentials are given which show the effect of cathode location and magnetic field.

Introduction

There still exist many unresolved questions concerning the operation of the MPD arc, directed primarily at the closely related problems of understanding arc acceleration mechanisms and optimizing performance of the MPD arc as a thruster. With respect to these problems, several parametric studies have been performed using selected combinations of the many variables which govern arc performance.[1,2,3,4,5,6] In a recent study relating plasma potential to variations in mass flow and dc magnetic field two of the authors found significant radial potential gradients extending several anode diameters into the exhaust of a 10-kw MPD arc.[4] On the basis of the results presented in reference 4, it was concluded that electromagnetic acceleration plays a significant role in arc performance and that such acceleration processes should be observable in the arc exhaust. Electrothermal effects have also been found but no assessment has been made of the efficiency of either mechanism in contributing to arc performance. In the present paper, using the same device described in reference 4, additional parametric variations are made which support the concept of a basically electromagnetic thruster. Results are presented for current, ion velocity, electron density, electron pressure, and potential distributions obtained with Langmuir, Hall effect, and magnetic probes.

Apparatus

10-kw MPD Arc

The 10-kw hollow-cathode porous-anode MPD arc used in this study is shown schematically in figure 1. A more detailed description is given in references 4 and 7. The applied magnetic field is slightly divergent and ranges from 700 to 2500 gauss, measured on the center line at the leading edge of the anode. The total gas flow used for all tests described in this paper is 10.2 mg of argon per second, divided evenly between anode and cathode in the manner described in reference 4. The device operates in a 5-foot-diameter by 15-foot-long vacuum facility capable of maintaining a background pressure of 0.2μ Hg under the present flow conditions. The pure tungsten hollow cathode of reference 4 has been replaced by a barium-impregnated tungsten tube which gives erosion-free operation over a wide range of power levels.

Probes

Construction details of Langmuir probes are shown in figures 2(a) and 2(b). For the probe of figure 2(a), iridium was chosen because its high work function minimizes thermionic emission. This probe is alined parallel to the flow and magnetic field axis and swept with a 60 Hz voltage signal. The current-voltage characteristic yields measurements of electron temperature T_e and, indirectly, plasma potential V_{pl}. The negatively biased rotating probe of figure 2(b) collects only ions and is based on the suggested use of such probes given in reference 8. It is motor-driven and oriented in the exhaust as shown in figures 3(a) and 3(b), (a) being the orientation for azimuthal velocity measurements and (b) for radial measurements.

Hall effect probes for magnetic field surveys have been constructed from commercially available sensors (F. W. Bell, Inc., models BH205 and BH206). Model BH206 is used for the current density measurements in this paper and the probe is shown in figure 4. The Hall effect probe, as well as both types of Langmuir probes, are driven radially and axially through the exhaust on a motor-driven boom at a speed of about 1 inch/sec.

A fourth diagnostic tool, for measurements of total azimuthal current, is a 200-turn magnetic pickup coil having an inside diameter of 2 inches. This coil has been either mounted directly onto the insulated anode face of the accelerator or driven axially along the center line of the exhaust. In use, the shutoff of the arc produces a time-changing flux which is first passively integrated and then amplified. The amplitude of the integrated signal is proportional to the azimuthal current. Characteristically, the shutoff time of the arc is 2 msec.

Experimental Results

Potential

Knowledge of the local distribution of plasma potential is important for understanding the types of acceleration mechanisms which exist in a particular accelerator. Briefly stated, the existence of equipotentials which are roughly perpendicular to magnetic field lines indicates an electrothermal expansion, while the presence of electromagnetic

effects is indicated by equipotentials which tend to be along magnetic field lines. (Of course, both types of acceleration can coexist in the same device.) The latter type of equipotential map has been found consistently in the present device for conditions tested to date.[4] It was felt that the overall dc power input to the device might affect the potential structure, as a basically similar low-power geometry[1] yielded equipotentials which indicated an electrothermal expansion. To test this possibility, the hollow cathode was extended forward until it was flush with the leading edge of the anode in the hope that potential troughs in the exhaust could be pushed as far downstream as possible. Such a geometry has no effect on the mode of arc operation - visual inspection shows that the cathode jet still comes from inside the hollow cathode and does not attach to the outer surface of the cathode. (However, such an attachment can be brought about under conditions of low power and very low cathode flow.) A comparison between high- and low-power operation is given in figure 5 (I_{arc} = 20 amperes, Power = 800 watts) and figure 6 (I_{arc} = 100 amperes, Power = 5000 watts). In figure 6, plasma potential evaluations are also given. Details of the correction of floating potential to plasma potential are given in reference 4. All potentials are referenced to the cathode. Because the data reduction system used in the reduction of Langmuir probe characteristics is intended for higher power operation (giving larger probe currents), a lack of sensitivity made the electron temperature values, and hence plasma potential, unavailable for figure 5 (low power). However, the shape and voltage level will be changed in about the same manner as in figure 6. In any event, the values given clearly show the existence of strong radial gradients for both conditions and there is no evidence to suggest that low-power operation has changed the basic potential structure of the arc.

With respect to the 300-watt arc of reference 1, it should be noted that the geometrical difference due to location of the cathode far back from the anode (even farther back than the normal cathode location of the present arc) may have as much significance as the power level which is still considerably lower than the 800-watt level tested in the hollow-cathode porous-anode arc. This possibility is presently under study.

Axial Current Density

The Hall effect probes described previously can be alined so that they measure only the magnetic field component produced by the axial current flowing in the accelerator exhaust. Then, taking $\mu_0 \vec{J} = \nabla \times \vec{B}$ in cylindrical coordinates, and assuming axial symmetry:

$$j_z = \frac{1}{\mu_0}\left(\frac{B_\theta}{r} + \frac{\partial B_\theta}{\partial r}\right)$$

Therefore, j_z can be calculated from a plot of B_θ vs. r. Such a computation has been carried out by computer using data obtained for several values of arc current and the results are shown in figure 7. The values for I_{arc} = 100 amperes at smallest z, given for completeness, are considered unreliable due to probe heating. It is immediately evident that a significant portion of the total arc current flows in the exhaust under all conditions. As with the potential surveys presented in the preceding section, there is no evidence to suggest that the lower-power arc is different in any significant way from the higher-power arc. For total arc currents of 50 amperes and lower, lack of sensitivity makes reliable measurements of B_θ increasingly difficult.

It is interesting to note that the magnetic field has little apparent effect on the level or shape of current density distributions in the exhaust. This conclusion has been supported consistently by other current density data obtained in the same device under a wide range of operation.

The total amount of current flowing at each z-value is given by integration:

$$I = \int j_z \, dA = 2\pi \int_0^R r j_z \, dr$$

where R is that value of r at which the current passes through zero. In cases where the overall level of current is high enough, the integration is continued to larger values of r to see if the total integrated current is zero, as it must be. Some integration has been carried out in all parts of figure 7 with results as shown.

A secondary effect noticeable in figure 7 is the apparent hole in the center of some of the distributions of j_z. It is not clear whether this represents a real characteristic of the exhaust or is brought about by the presence of the relatively large probe. Repeating the measurement with a smaller probe has produced equally inconsistent results close to r = 0, so that the measurement has not been proven independent of the probing device (although larger values of r yield similar data for both probes). Nonetheless, there is reason to suspect that there can in fact be a hole in the distribution of j_z - this will be discussed in conjunction with other measurements in "Discussion of Experimental Results."

Ion Velocity

In principle, the directed ion velocity can be obtained from a rotating negatively biased Langmuir probe, such as described in figures 2(b) and 3 by separating the velocity from the particle current $n\vec{v}$ collected by a negatively biased probe in a high-speed flow.[8] However, computation of the absolute magnitude of the ion velocity (which is on the order of 10^4 m/sec) is complicated even with probe geometries for which theory is adequate[9] - the flat probe surface used here is not such a geometry. Therefore, the present study is limited to obtaining the direction of the velocity vector in the r - z and θ - z planes. The rotating probe is oriented and driven through the plasma exhaust as shown in figure 3. For one measurement, $\vec{v}_r$ is always parallel to the probe surface (and not collected) and for the other, $\vec{v}_\theta$ is parallel. Assuming that n is constant in the vicinity of the probe, the direction of $\vec{v}_{rz}$ or $\vec{v}_{\theta z}$ is found simply by searching for the maximum ion current on each revolution and calculating its

angular orientation. Figure 8 shows results of such calculations for $\vec{v}_{rz}$ and figure 9 for $\vec{v}_{\theta z}$. The angle of the velocity vector is zero in the r - z or θ - z plane for a purely axial vector. Definition of positive or negative direction is arbitrary. The first figure shows a radially outward ion divergence which increases approximately linearly with r at given z and decreases with increasing z at given r. A significant difference between high and low field, indicating increased confinement for higher field, is evident only in figure 8(c).

Figure 9, dealing with azimuthal velocity, shows in each case the conversion of rotation into translation, although nothing can be said about the magnitude of $\vec{v}_{\theta z}$. Further comments on interpretation of these velocities will be included in "Discussion of Experimental Results." The radial zero shift apparent in all the azimuthal velocity curves represents a consistent error due to gear backlash in the driving mechanism.

Azimuthal Current

There are two common methods for using magnetic probes to measure azimuthal currents. The simpler of the two uses a magnetic pickup coil which encircles the exhaust and responds to all time-changing azimuthal current in its vicinity. The other, the Rogowski coil, can be made responsive only to that time-changing current which actually threads the loop formed by the coil. Because of size limitations and a poor signal-to-noise ratio, the Rogowski coil so far has not produced reliable measurements. However, a magnetic pickup coil, used as described in "Apparatus," has shown that the total azimuthal current flowing in the arc is at least an appreciable fraction of the total arc current. Despite the fact that the current so defined cannot be assigned a particular spatial distribution or magnitude, even a qualitative assurance of its existence has considerable significance, as it is required for plasma containment regardless of whether electromagnetic or electrothermal acceleration is taking place.

Density and Electron Pressure Measurements

The previous discussions pertaining to observed electromagnetic effects should not be taken as implying that electrothermal effects are not present in the hollow-cathode porous-anode arc. Figure 10 shows a typical distribution of electron density and figure 11 gives the corresponding distribution of electron pressures computed from figure 10 and previously obtained electron temperature surveys. The arc conditions given are similar to those of other data in this paper. The cathode is in the normal location, as shown in figure 1. A simple calculation of the axial electrothermal expansion field in units of volts/inch, $\nabla P_e/n_e e$, suffices to show that electrothermal effects are comparable with electromagnetic effects in some regions. Figure 12 shows values of the axial electrothermal fields at r = 0 and r = 1/2 inch computed from the pressure plots of figure 11 and corresponding electric fields computed from plasma potential profiles (the potential profiles themselves are not included here). At r = 0, the two fields are comparable, whereas off axis, at r = 1/2 inch, the electric fields, both axial, as shown here, and radial, predominate. It should be emphasized that values given for these z-fields are subject to considerable uncertainty, as the evaluation of axial gradients from just a few points is only an approximate procedure.

The balancing, within available accuracy, of electric and electrothermal fields at r = 0 has significance in comparison with axial current density measurements, as will be discussed in the following section.

Discussion of Experimental Results

Evidence of Electromagnetic Acceleration in the Plasma Exhaust

The basic experimental evidence which confirms the existence of electromagnetic effects in the exhaust of the present device are the consistently observed potential gradients and axial currents discussed previously in this paper and in reference 4. Observation of the conversion of ion rotation into translation in the exhaust can be explained either by axial electromagnetic acceleration in the exhaust (since there is still energy being added to the plasma as the result of currents and fields) or by conservation of angular momentum in the case where currents are confined to the electrode region. The rather scattered data of figure 9 cannot provide enough information to separate these effects, but it is clear that at the closest z-value measured (2 anode diameters) the ions have an azimuthal velocity component of at least 30° which must be produced by electromagnetic forces acting somewhere in the device, and that this component decreases (in percentage of the total velocity) in regions where axial electromagnetic forces are made plausible by currents and fields known to exist. These forces are, specifically, $j_r B_\theta$ and $j_\theta B_r$ Lorentz forces per unit volume. Inasmuch as the behavior of the magnitude of v_θ is not known, the efficiency of the electromagnetic acceleration cannot be evaluated on the basis of the data presented here.

Measurements made with ion-collecting Langmuir probes of the type in figure 2(a) show that the rotation of ions may not correspond to ion motion in a uniform plasma, but may result from rotation of a nonuniformity in the plasma. An azimuthal ion velocity orientation of 30° with respect to the axis represents an order-of-magnitude speed of about 5000 m/sec based on an axial velocity of 10^4 m/sec. The rotational frequency which such a velocity predicts is well within the range of phenomena observed by other experimenters. (One such reference is a companion paper by Brockman, et al., presented at this conference.) For a 1-inch-diameter anode, an expected frequency is about

$$\left(\frac{1}{5 \times 10^{-2}} \text{ rev/meter}\right)(5000 \text{ m/sec}) \approx 10^5 \text{ rev/sec}$$

Possible Divergence of Axial Currents

As noted previously in the section dealing with axial current, there is an indication of a hole in the axial current densities near r = 0 as shown in figure 7. Considering that even the smallest B_θ probe used is 10 percent of the total anode diameter (although the sensing area itself is much smaller), this effect is difficult to clarify. If real, this hole would mean that the axial current is somewhat divergent, following magnetic field

lines. Such a behavior would not be unreasonable, and it is made likely by the comparative size of electrothermal gradients and electric fields such as those of figure 12. Since at $r = 0$ the pressure and electric field terms are about the same size and opposite in sign, there should be little or no axial current at $r = 0$, i.e.,

$$j_z = \sigma\left[E_z + \left(\frac{\nabla P_e}{n_e e}\right)_z\right]_{r=0} \approx 0$$

while at $r = 1/2$ inch, the electric fields, both radial and axial, predominate and are large enough to produce the observed current density for reasonable values of σ.

MPD Arc Simulation With Low-Power Devices

All the experimental data taken so far at low power show the structure of the exhaust beam to be substantially the same as for higher power levels. This gives an obvious advantage in local diagnostics, especially Langmuir probe studies, because detailed surveys can be made close to the electrodes in a true MPD arc device. The advantage with respect to current density in terms of less probe heating is somewhat offset by a loss in sensitivity as the B_θ field produced by smaller j_z approaches unmeasurable values. The lower limit of input power at which MPD arc operation is maintained in the hollow-cathode porous-anode device has not been accurately established.

No complete parametric surveys of MPD arc operation have yet been made at low power in the device used here, although such studies may prove useful as an alternative to operating high-power devices in the pulsed mode - requiring an order-of-magnitude increase in the complexity of gas feed systems and diagnostic instrumentation.

Computer Calculations of Potential Distributions in the Exhaust of an MPD Arc

Using electrode configurations similar to those of the acclerator used for the experiments described previously, difference equation solutions have been obtained for several values of magnetic field and cathode location. The calculations have a twofold purpose: (1) To see if qualitative agreement can be obtained with experiment even when a considerable number of restrictive assumptions are made, and (2) to check the influence of boundary value selection on the accuracy of the solutions.

The method of solution is similar to that in reference 10. The divergence of Ohm's Law is taken:

$$\nabla \cdot \vec{j} = \nabla \cdot \left(\overleftrightarrow{\sigma}\,\vec{E}\right) = -\nabla \cdot \left(\overleftrightarrow{\sigma}\,\nabla\varphi\right) = 0$$

This results in a second-order elliptic differential equation. The assumptions made are that $\vec{B} = \hat{k}B_z = \text{Constant}$, σ_o, n_e, τ_i, τ_e, T_e, and T_i are constant, and that no center of mass velocities are present. The resulting equation is

$$\beta\left(\frac{\partial^2\varphi}{\partial r^2} + \frac{1}{r}\frac{\partial\varphi}{\partial r}\right) + \frac{\partial^2\varphi}{\partial z^2} = 0$$

where

$$\beta = \frac{1 + 2f^2\omega_e\tau_e\omega_i\tau_i}{1 + \left(\omega_e\tau_e\right)^2 + \left(1 + 2f^2\omega_i\tau_i\omega_e\tau_e\right)\left(2f^2\omega_e\tau_e\omega_i\tau_i\right)}$$

and f is the percentage of unionized neutrals. The equation is solved by a five-point difference equation method[11] on a 30×30 grid of points $1/8$ inch apart. Anode potential is set at +1 and cathode potential at zero. All other boundaries are insulators.

In order to check the accuracy of solutions, different initial values were set on the boundaries to start the iteration. It was found that, for example, using $\beta = 0.01$ (high magnetic field) and accuracies as high as 0.0001 for each calculation, the cumulative error for each calculation tended to add so that the solution converged on the original initial value set at the outer insulating wall. With an accuracy of 0.00001 it was possible to have two solutions - one for an initial value of 0.5 and another for 1.0 - converge on the same values within 10 percent at the outer boundaries. This relatively simple case required over 10 minutes of CDC 6600 time.

In figure 13, four extreme cases are presented using $\beta = 0.01$ (high field) and $\beta = 1$ (zero magnetic field) with long and short cathodes. These figures show the same trends as observed experimentally in this paper and in reference 4, namely, that moving the cathode forward tends to force equipotentials downstream, and that increasing B tends to make equipotentials follow B more closely, i.e., equivalently, increasing $\vec{E}_r$ at a given value of z.

Conclusions

It is concluded that the accelerator used for these tests is basically an electromagnetic device, although electrothermal effects have been observed and no measure is available for assessing the relative efficiencies of either type of acceleration. This conclusion is supported by the existence of plasma potential gradients and axial currents several anode diameters into the exhaust. In addition, conversion of ion rotation into translation has been observed in the exhaust. Verification of the existence of a large azimuthal current of unknown distribution and magnitude has satisfied our expectations, although it has yielded no quantitative information.

Computer solutions of Laplace's equation have shown that because of slow convergence, initial boundary values must be chosen with care to avoid excessive computing time. The computer solutions for plasma potential show qualitative agreement with experimentally observed behavior.

Acknowledgement

We wish to express appreciation to Lillian Boney of Langley who programed the numerical solutions to Laplace's equation.

References

1. Bowditch, D. N.: Investigation of the Discharge and Exhaust Beam of a Small Arc Plasma Thrustor. AIAA Plasmadynamics Conf., Monterey, Calif., Mar. 2-4, 1966. AIAA Paper No. 66-195.

2. Burlock, J.; Brockman, P.; Hess, R. V.; and Brooks, D. R.: Measurement of Velocities and Acceleration Mechanism for Coaxial Hall Accelerators. AIAA J., vol. 5, no. 3, Mar. 1967.

3. Cann, G. L.; Harder, R. L.; Moore, R. A.; and Lenn, P. D.: Hall Current Accelerator. EOS Rept. 5470, Feb. 4, 1966.

4. Hoell, J. M.; and Brooks, D. R.: Effect of Propellant Injection Through Electrodes on Potential Distribution in an MPD Arc. AIAA 5th Aerospace Sci. Meeting, New York., AIAA Paper No. 67-49, Jan. 23-27, 1967.

5. Patrick, R. M.; and Schneiderman, A. M.: Axial Current Distribution in the Exhaust of the Magnetic Annular Arc. Avco-Everett Research Lab., Res. Rept. 231, July 1966.

6. Powers, William E.: Measurements of the Current Density Distribution in the Exhaust of an MPD Arc Jet. AIAA 3rd Aerospace Sci. Meeting, New York, Jan. 24-26, 1966.

7. Weinstein, R. H.; and Hoell, J. M., Jr.: Experiments in a Hollow Cathode Hall Current Accelerator: AIAA 2nd Annual Meeting, San Francisco, July 26-29, 1965. AIAA Paper No. 65-299.

8. Brooks, D. R.: Use of Rotating Langmuir Probes in Flowing Plasmas: Rev. Sci. Instr., vol. 37, no. 12, Dec. 1966.

9. Laframboise, J. G.: Theory of Spherical and Cylindrical Langmuir Probes in a Collisionless, Maxwellian Plasma at Rest. Inst. for Aerospace Studies, Univ of Toronto, UTIAS Rept. No. 100.

10. Coleman, R. L.; Hassan, H. A.; and Garcia, B. H.; Jr.: Potential and Current Distributions in MPD Arcs. AIAA 5th Aerospace Sci. Meeting, New York, Jan. 23-26, 1967. AIAA Paper No. 67-48.

11. Starling, P. P.: The Numerical Solution of Laplace's Equation. Brit. J. Appl. Phys., vol. 14, 1963.

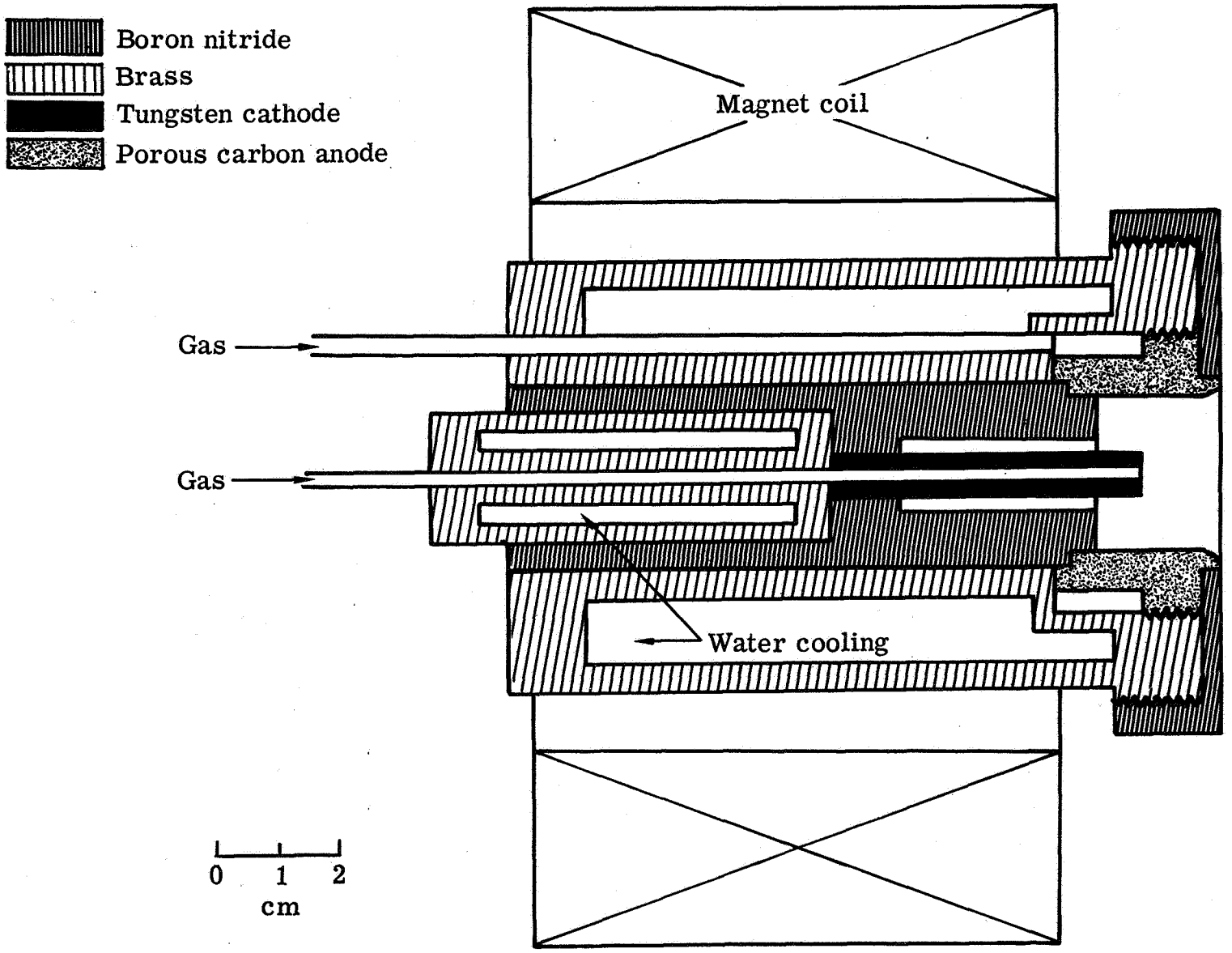

Figure 1.- Hollow cathode–porous anode arc jet.

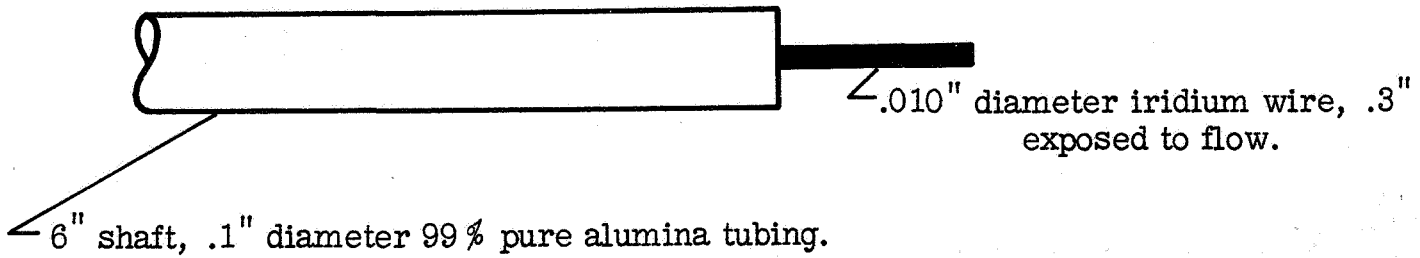

(a) T_e and V_{pl} probe.

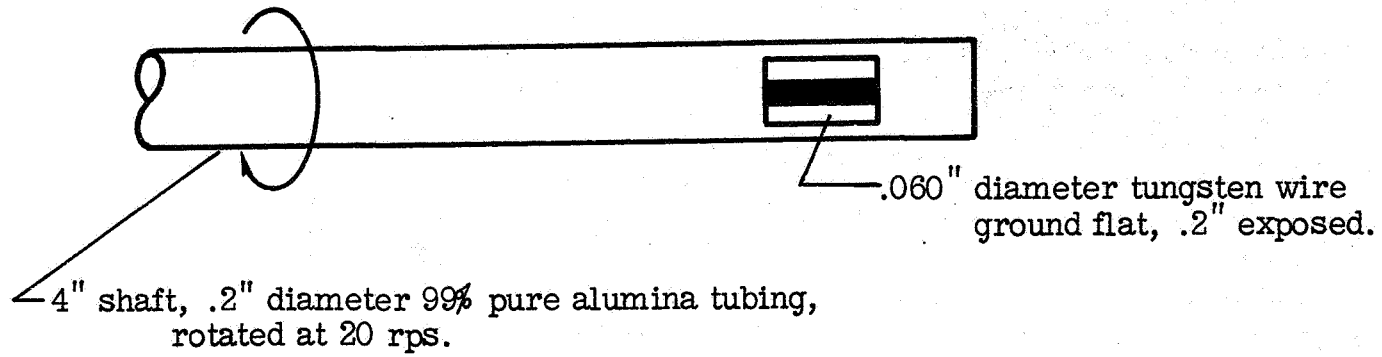

(b) Negatively biased rotating probe.

Figure 2.- Langmuir probe construction details.

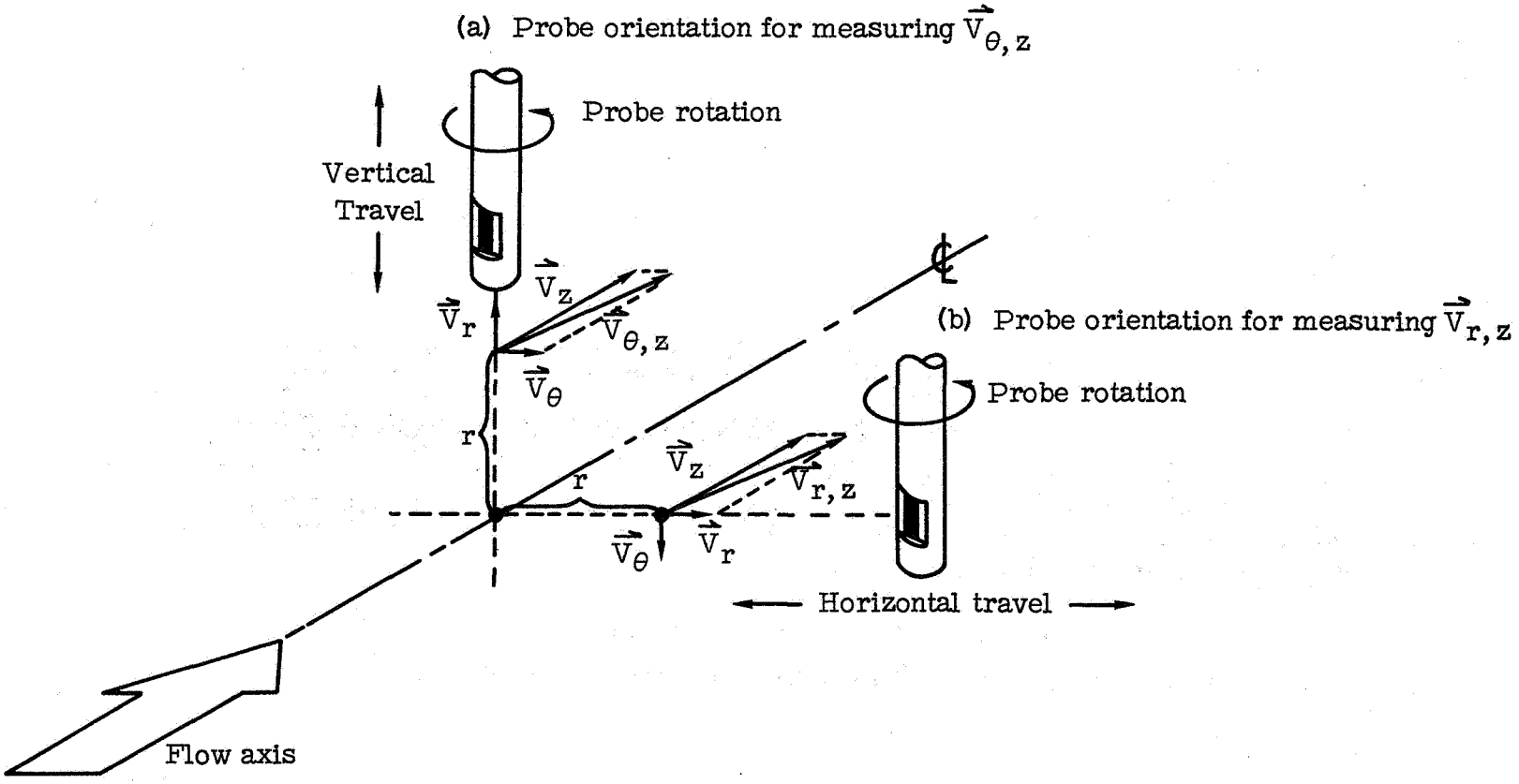

Figure 3.- Orientation of rotating probe for determination of $\vec{V}_{\theta,z}$ and $\vec{V}r,z$.

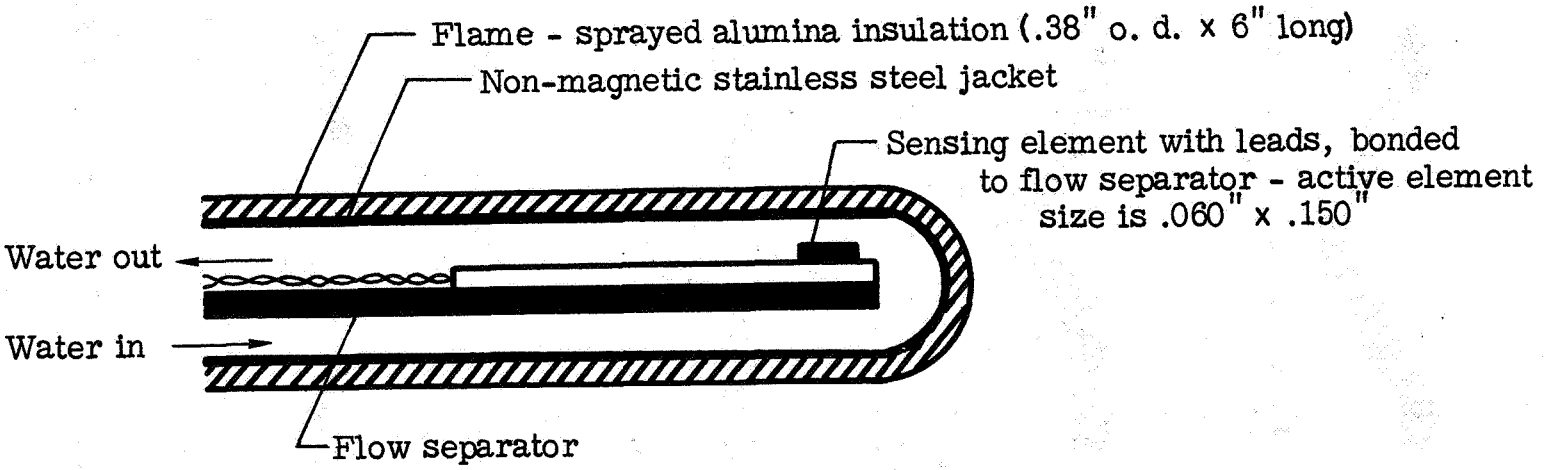

Figure 4.- Construction details of water-cooled Hall effect probe.

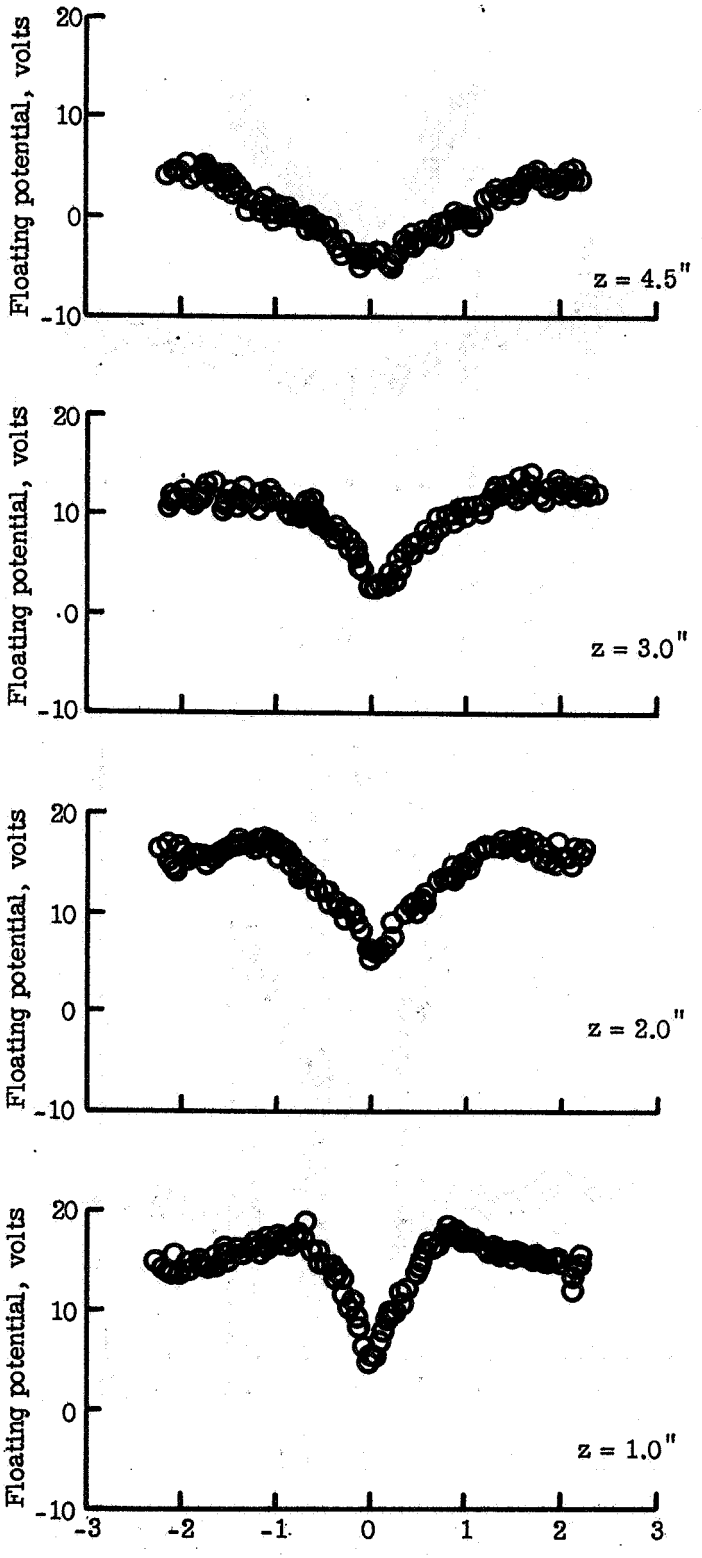

Figure 5.- Floating potential measurements for 800 W input power. I_{arc} = 20A, B = 700G.

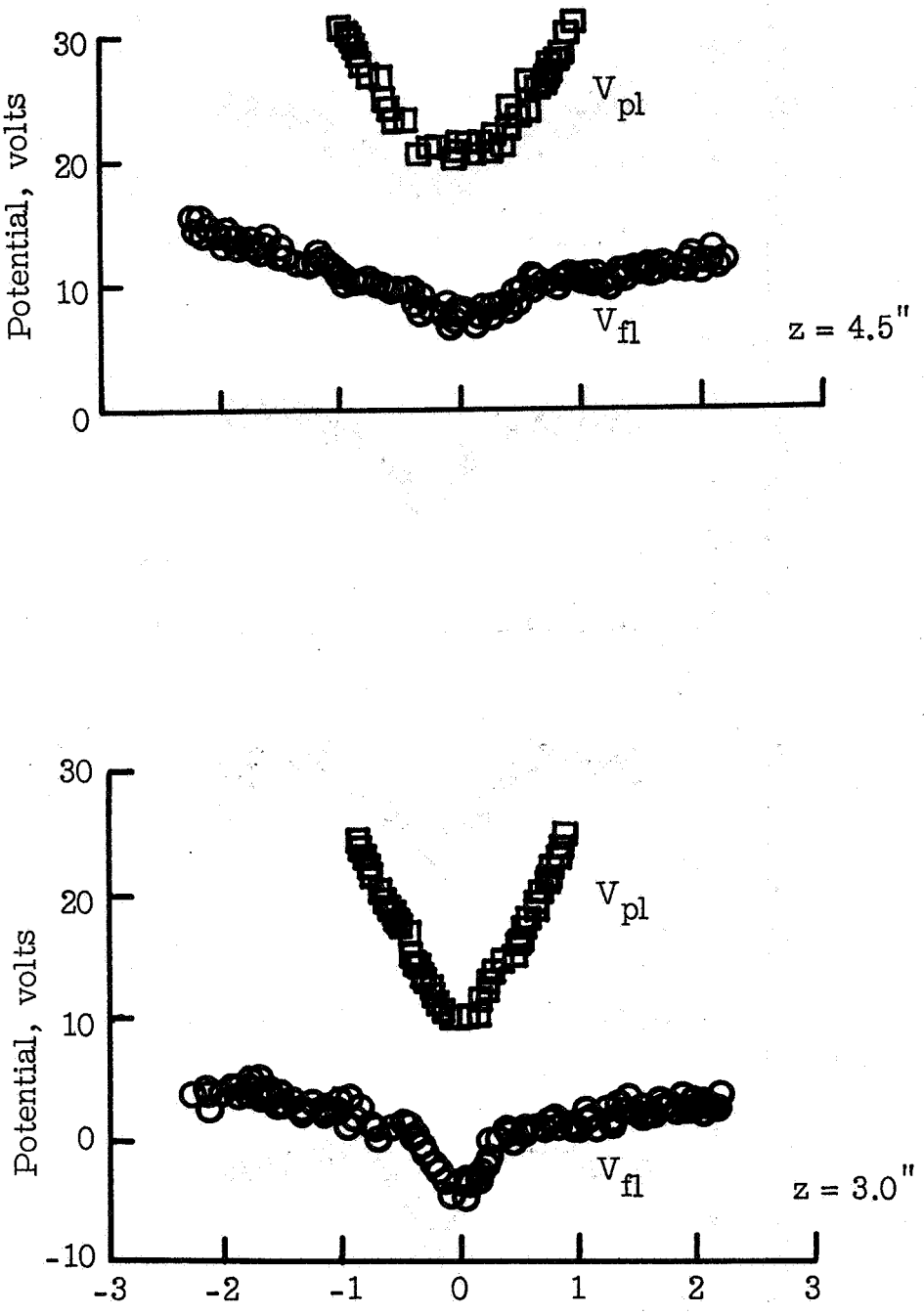

Figure 6.- Floating potential and plasma potential measurements for 5000 W input power. I_{arc} = 100A, B = 700G.

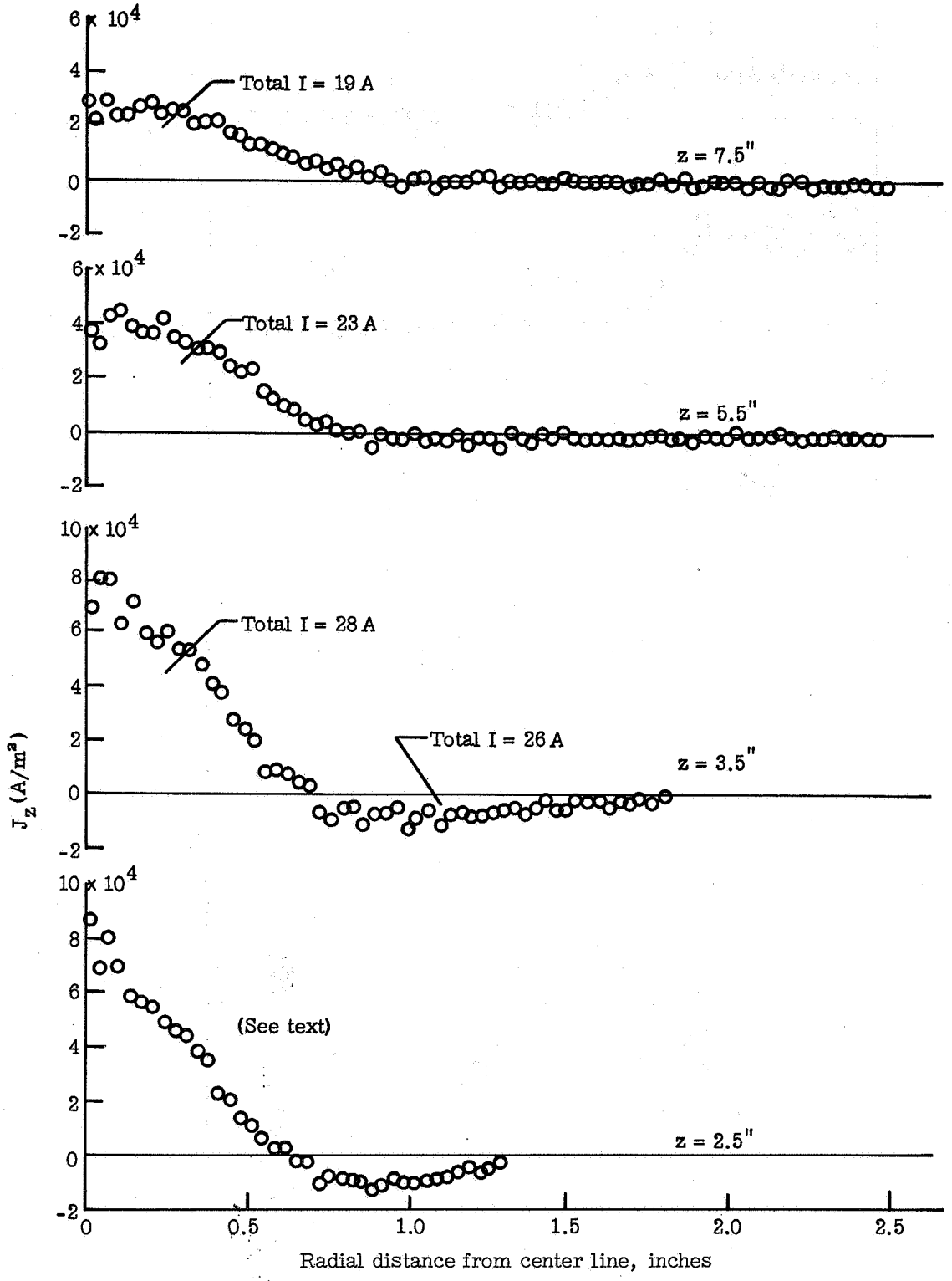

(a) I_{arc} = 100 A, B = 700 G

Figure 7.- J_z as a function of r and z.

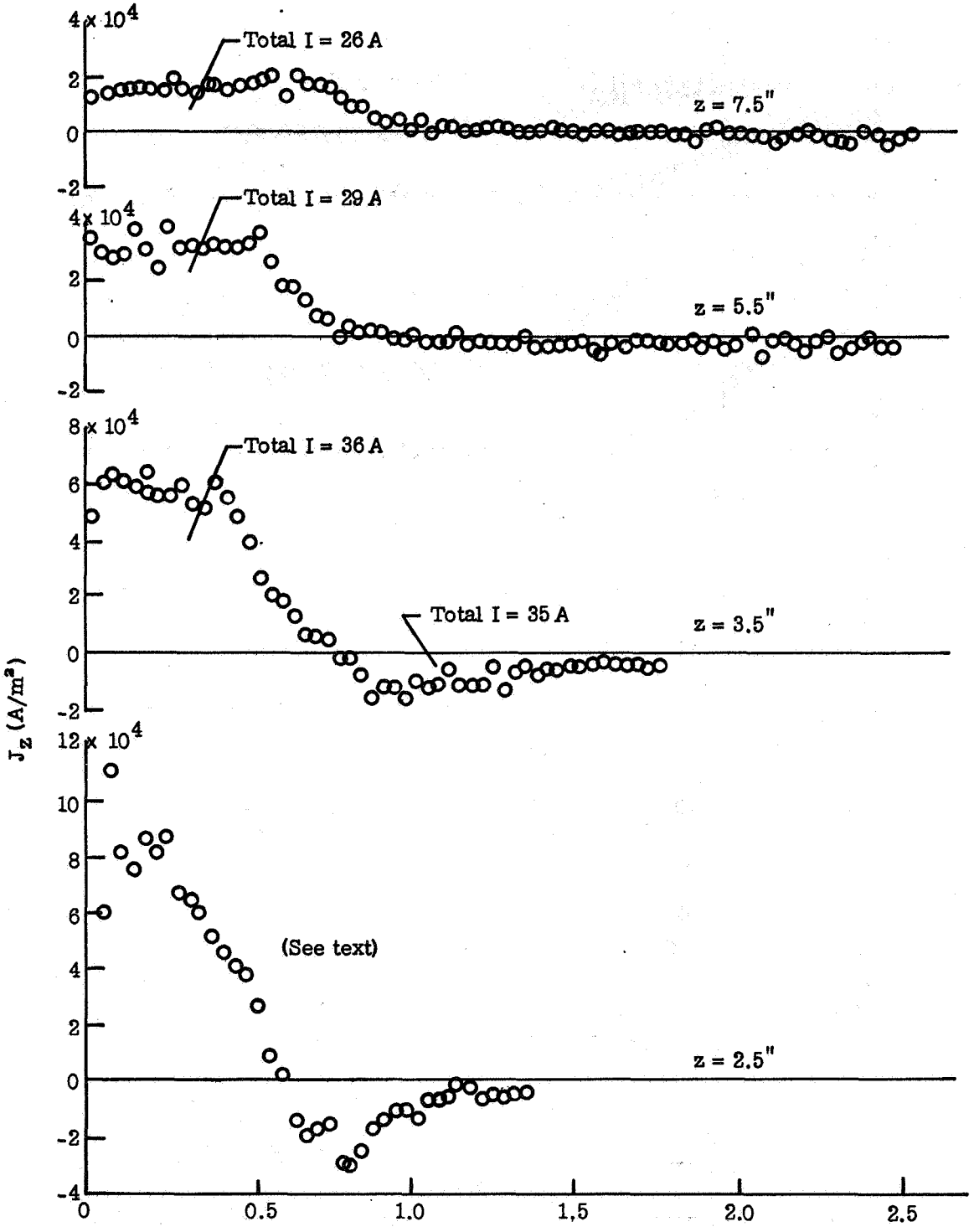

(b) I_{arc} = 100 A, B = 2500 G

Figure 7.- Continued.

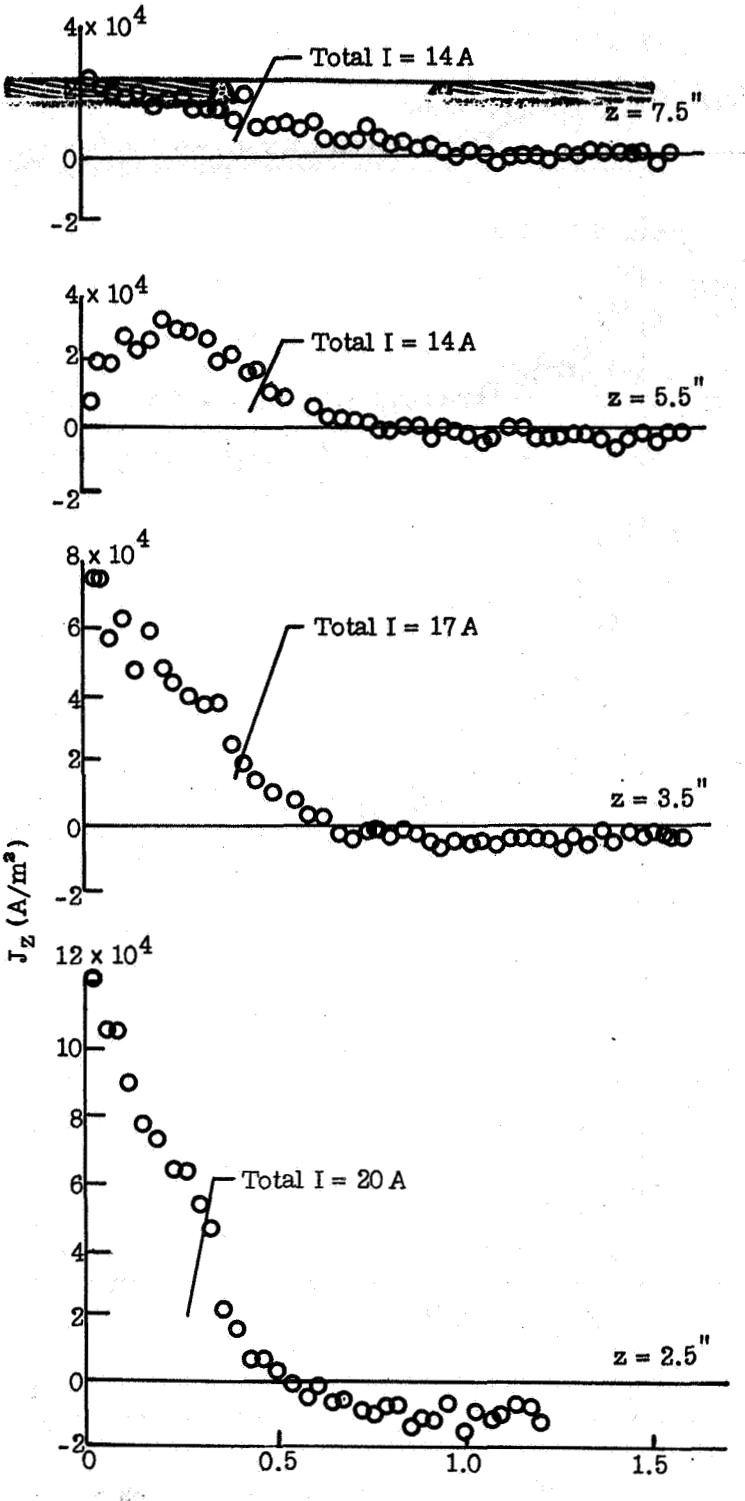

(c) I_{arc} = 50 A, B = 700 G

Figure 7.- Continued.

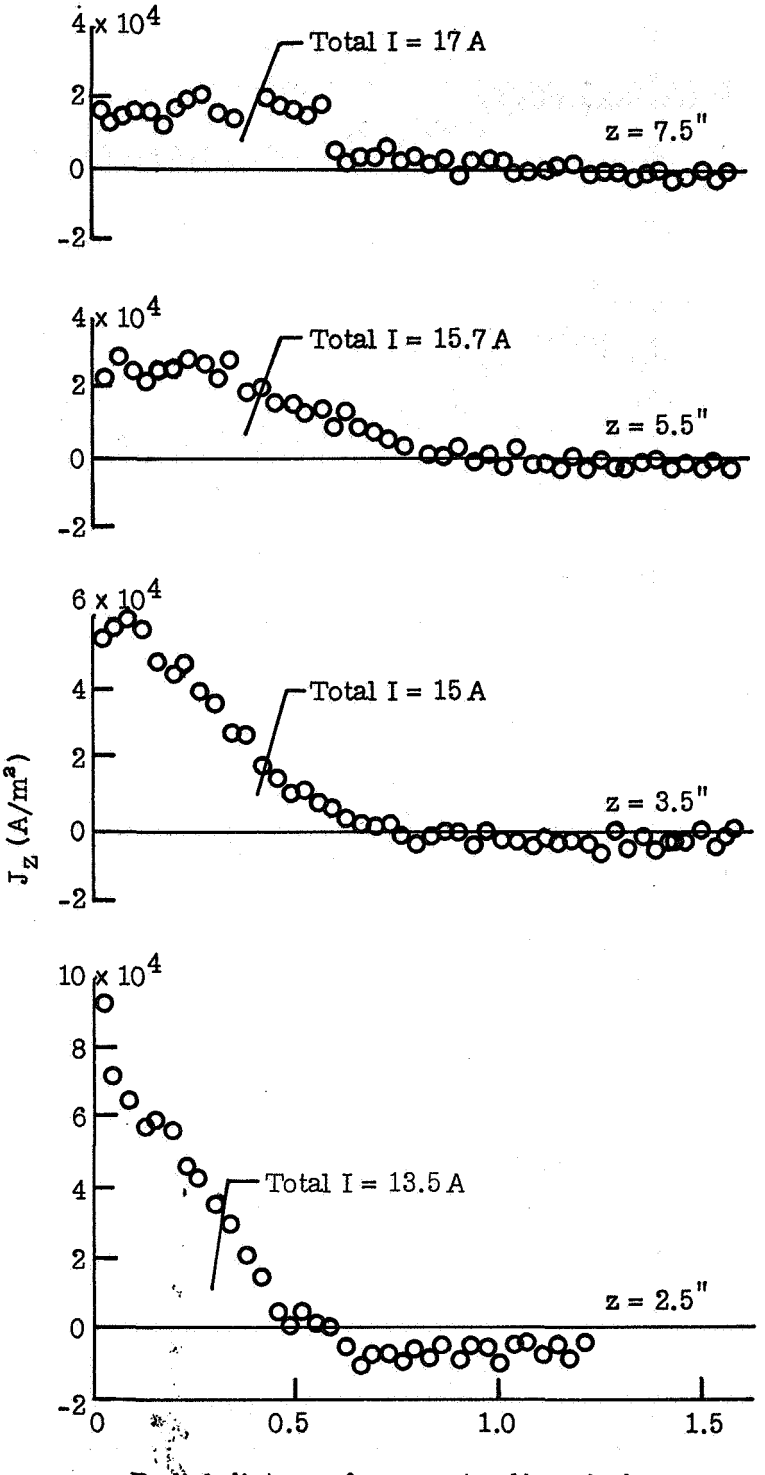

(d) I_{arc} = 50 A, B = 2500 G

Figure 7.- Concluded.

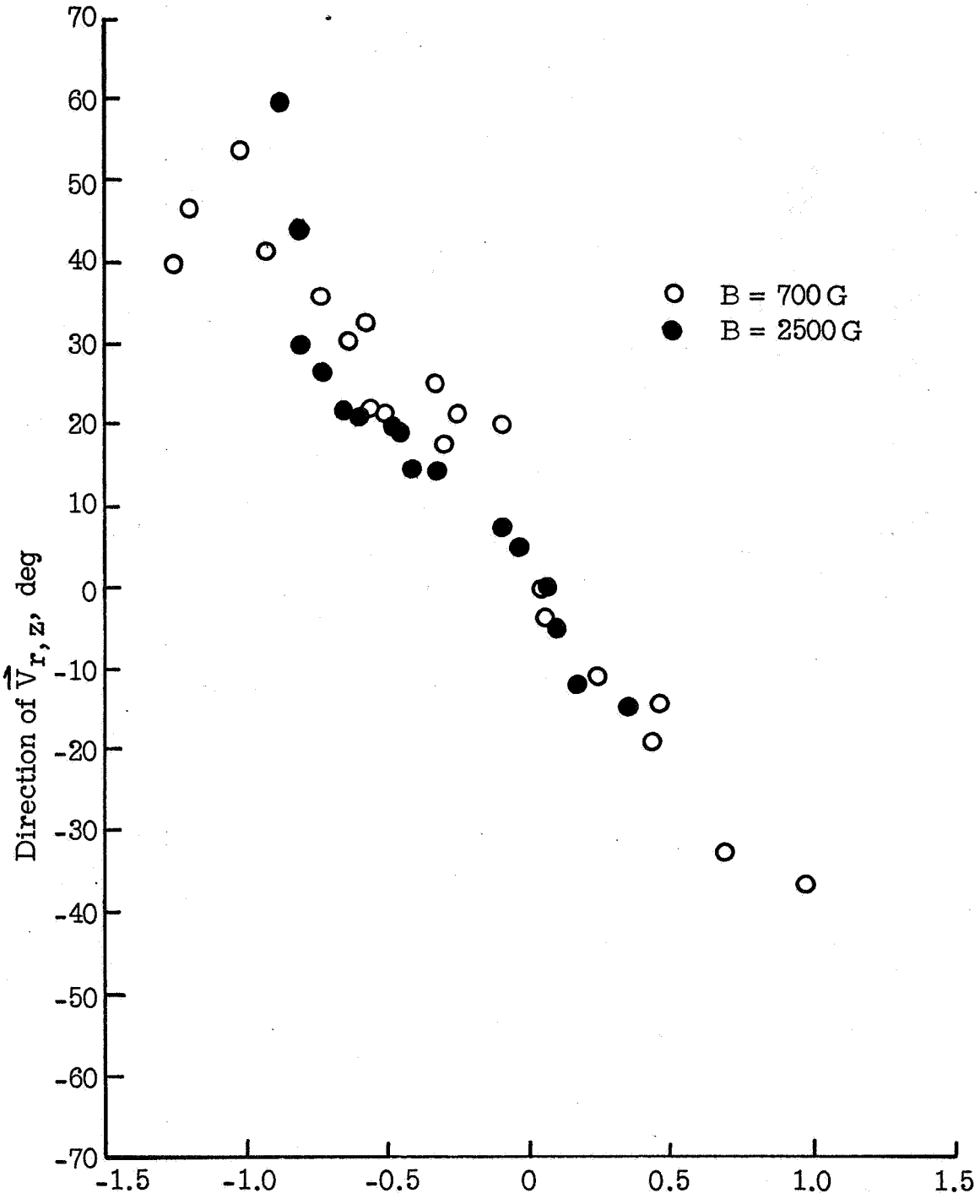

(a) $I_{arc} = 100$ A, $z = 2.0$"

Figure 8.- Direction of $\vec{V}_{r,z}$.

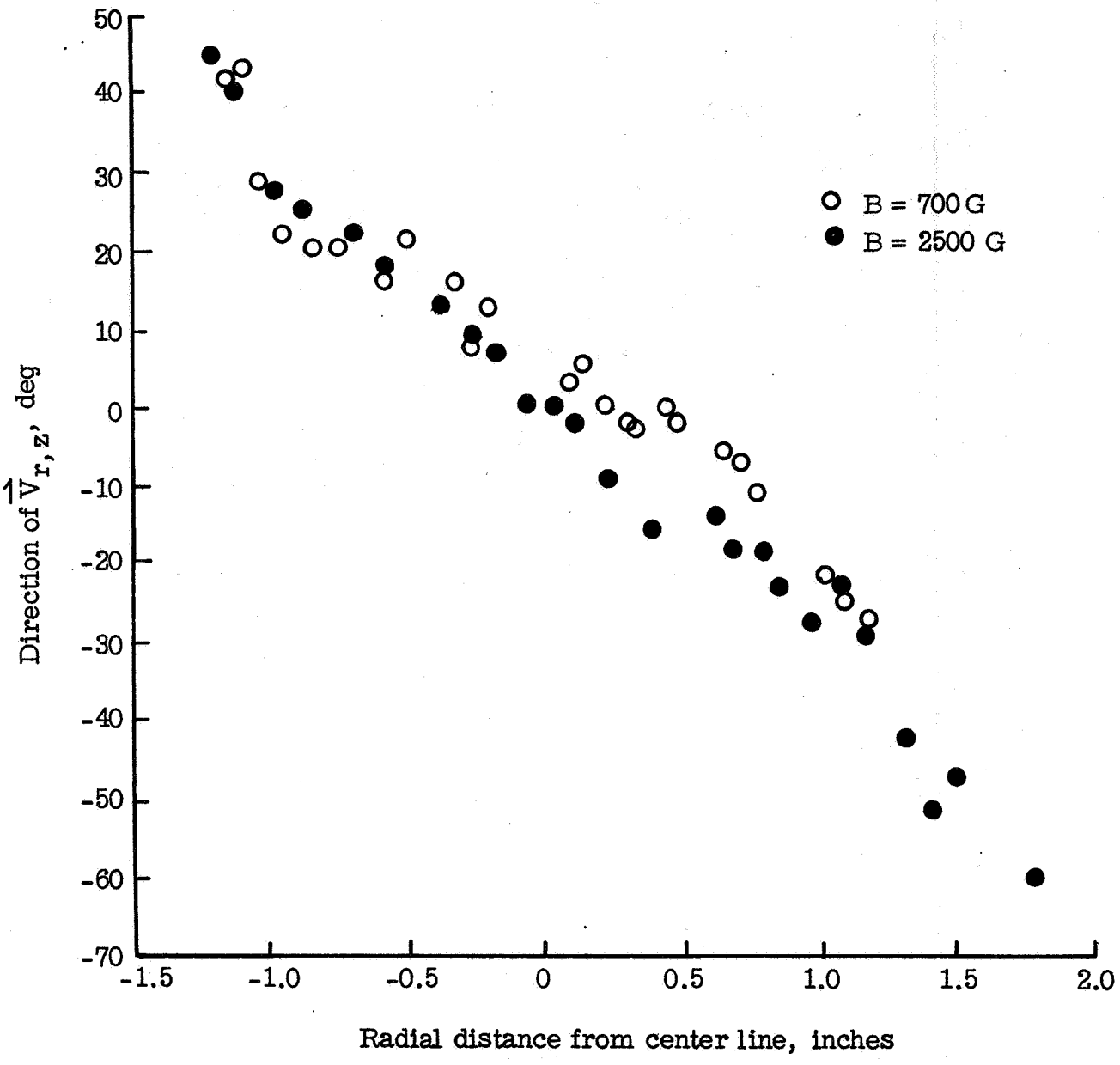

(b) I_{arc} = 100 A, z = 3.0"

Figure 8.- Continued.

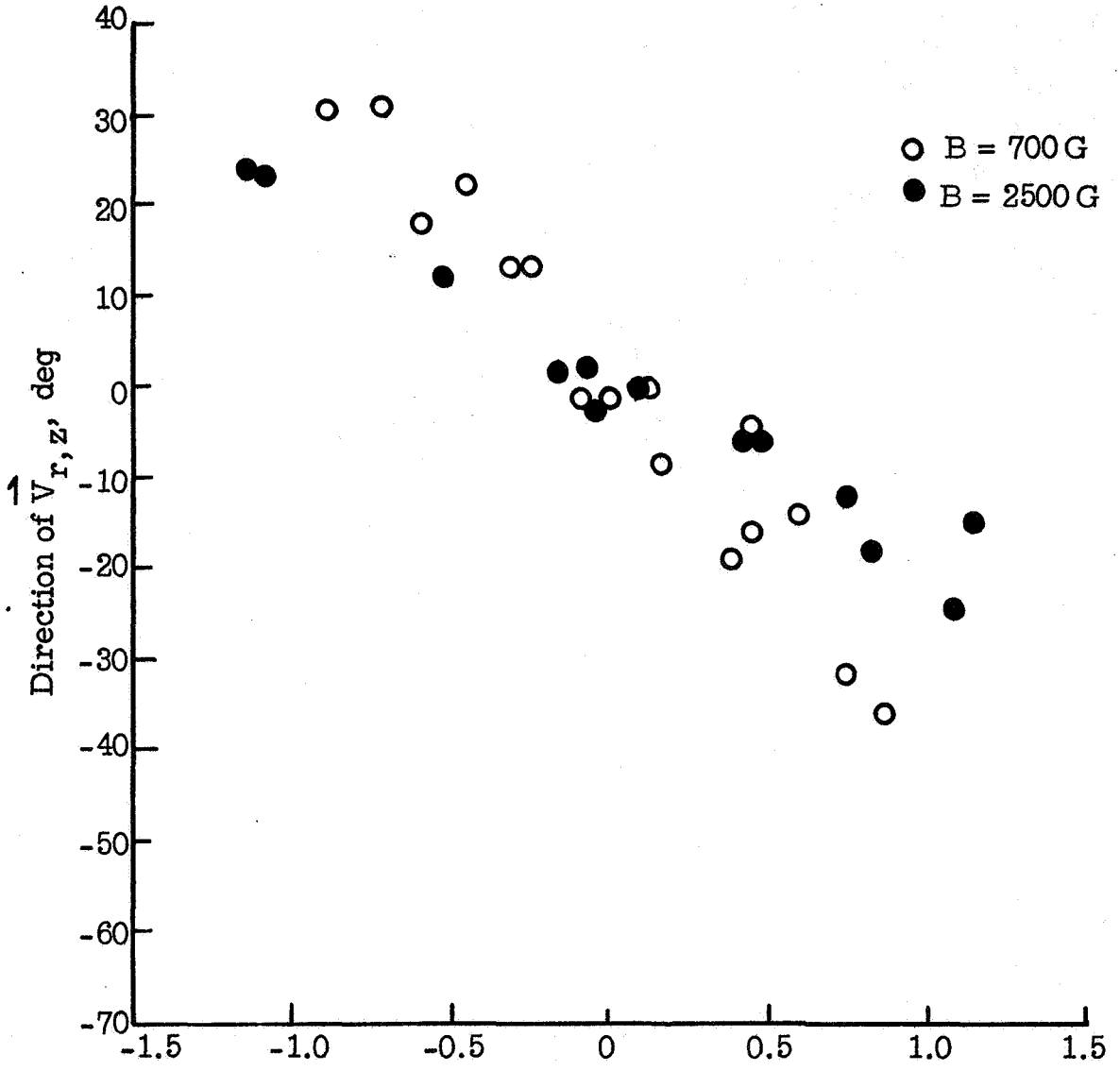

(c) I_{arc} = 100 A, z = 4.0"

Figure 8.- Continued.

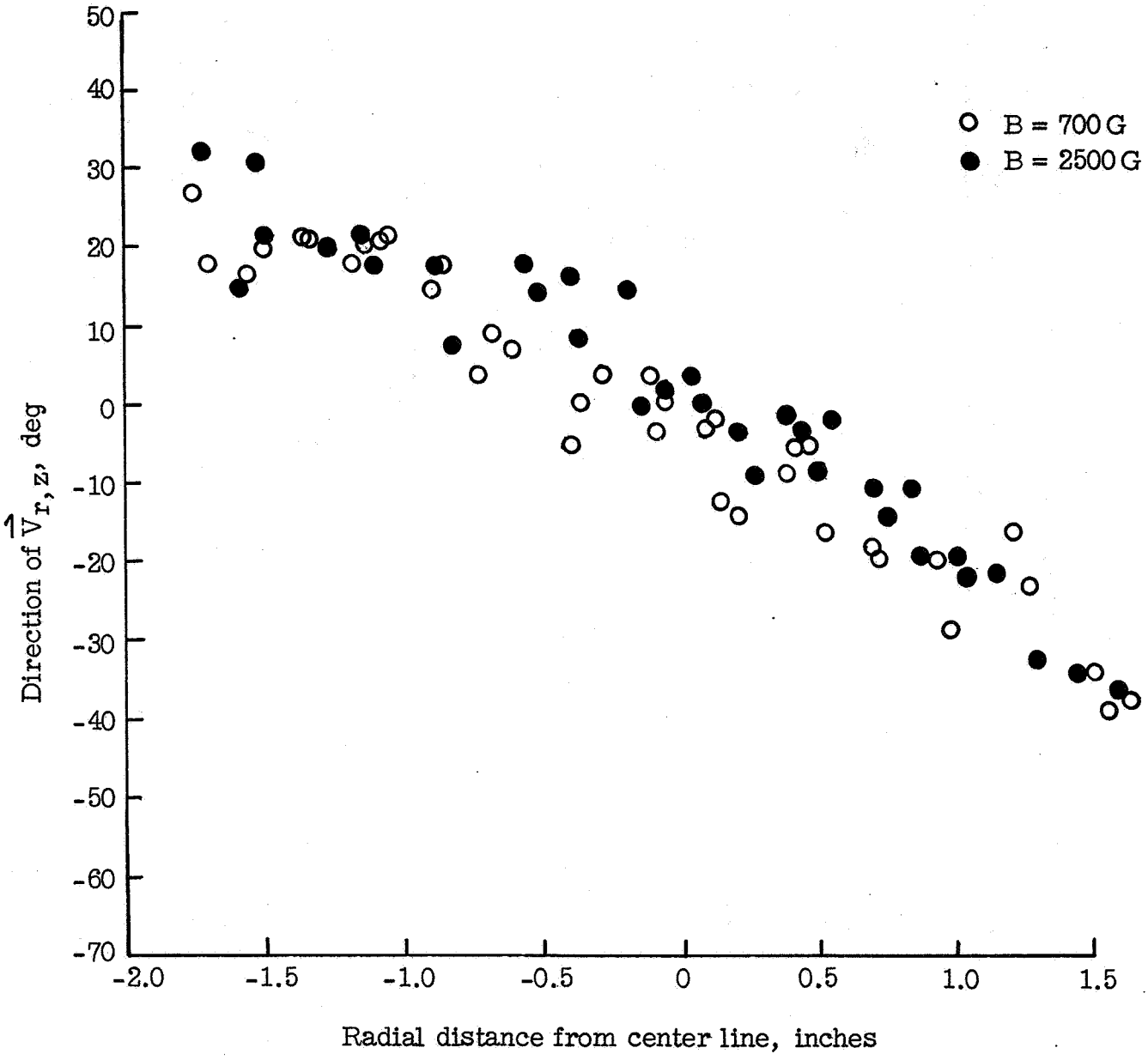

(d) I_{arc} = 100 A, z = 6.0"

Figure 8.- Concluded.

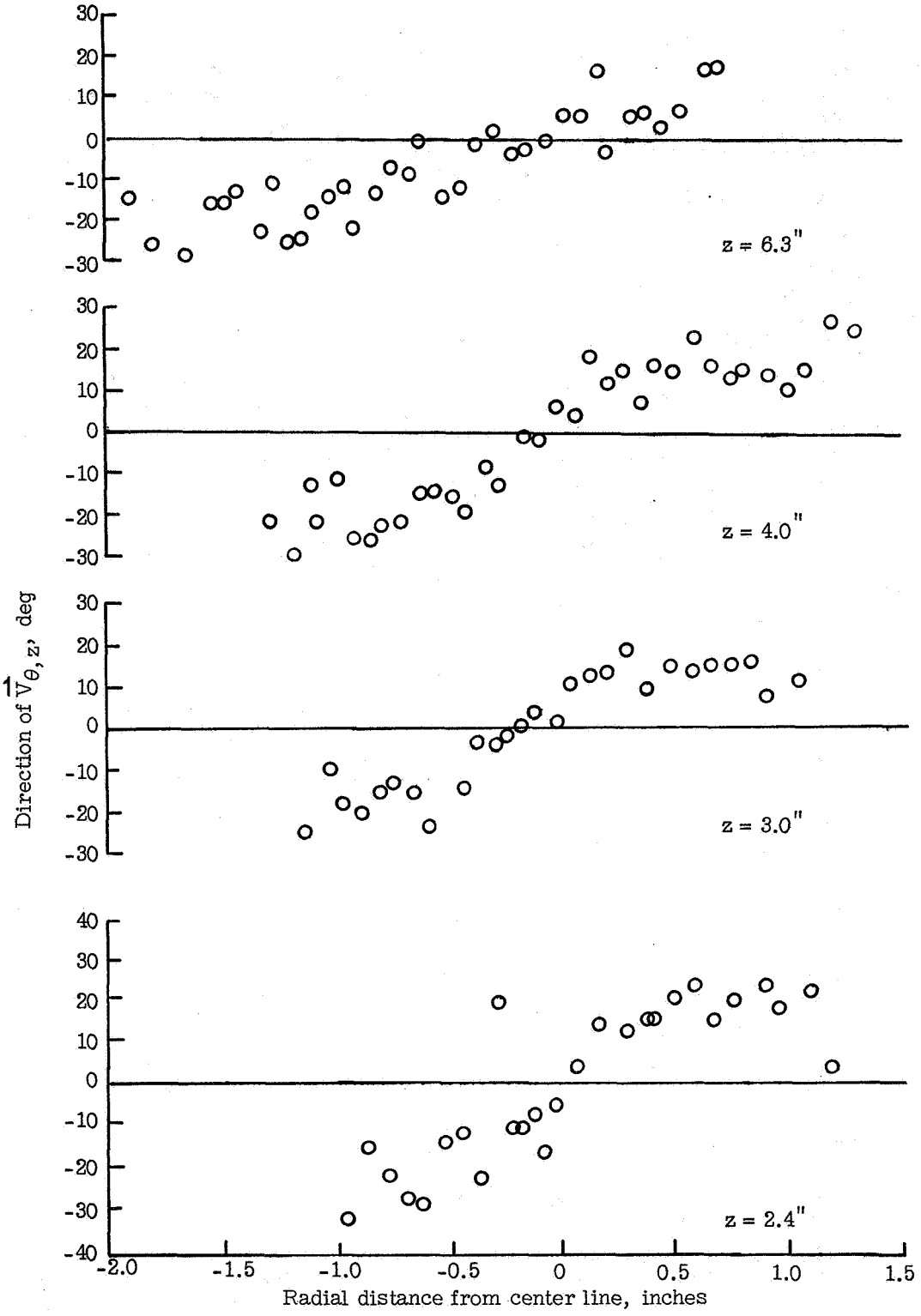

(a) High current, low field. I_{arc} = 100 A, B = 700 G

Figure 9.- Direction of $\vec{V}_{\theta,z}$.

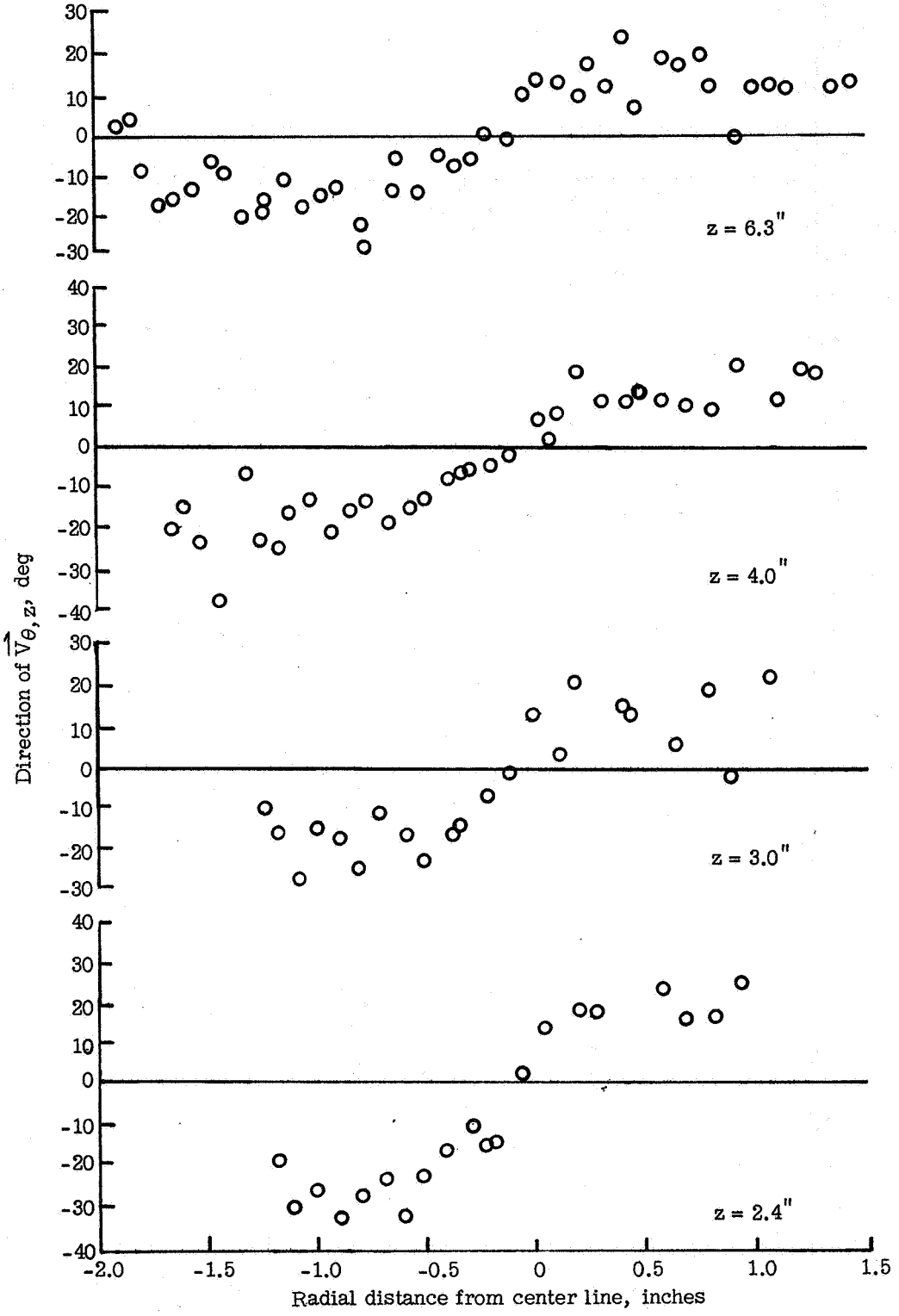

(b) High current, high field. I_{arc} = 100 A, B = 2500 G

Figure 9.- Continued.

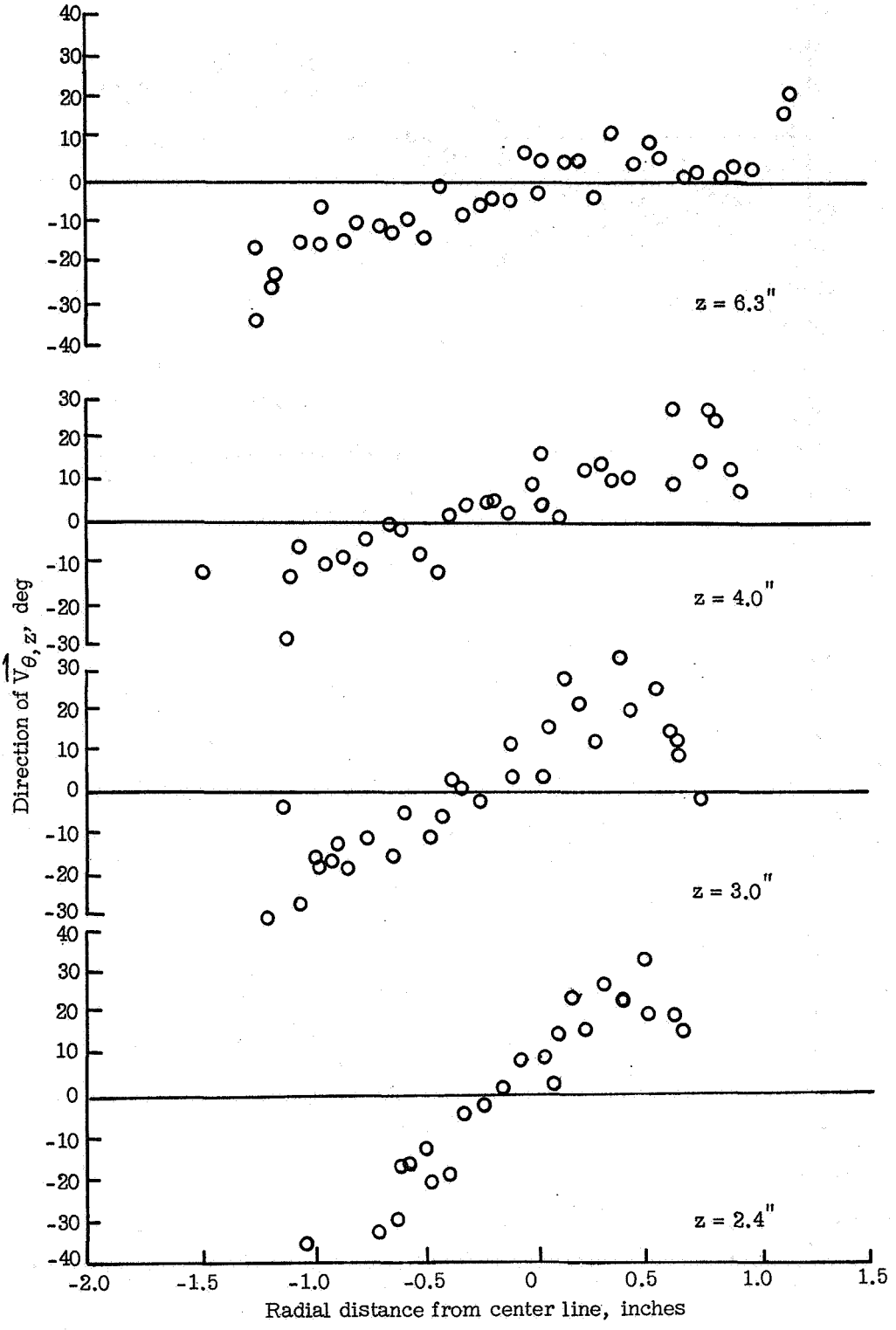

(c) Low current, low field. I_{arc} = 50 A, B = 700 G

Figure 9.- Continued.

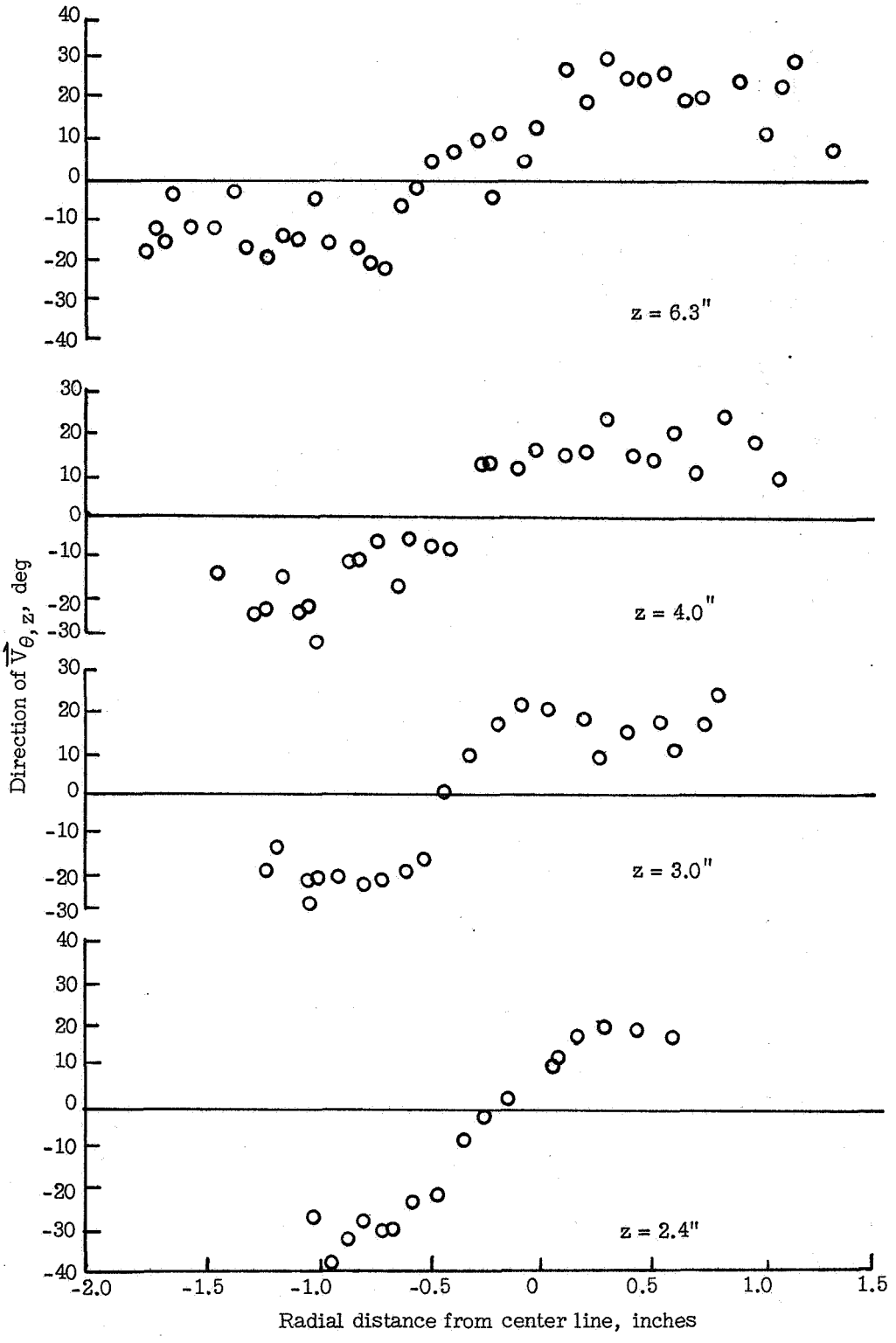

(d) Low current, high field. I_{arc} = 50 A, B = 2500 G

Figure 9.- Concluded.

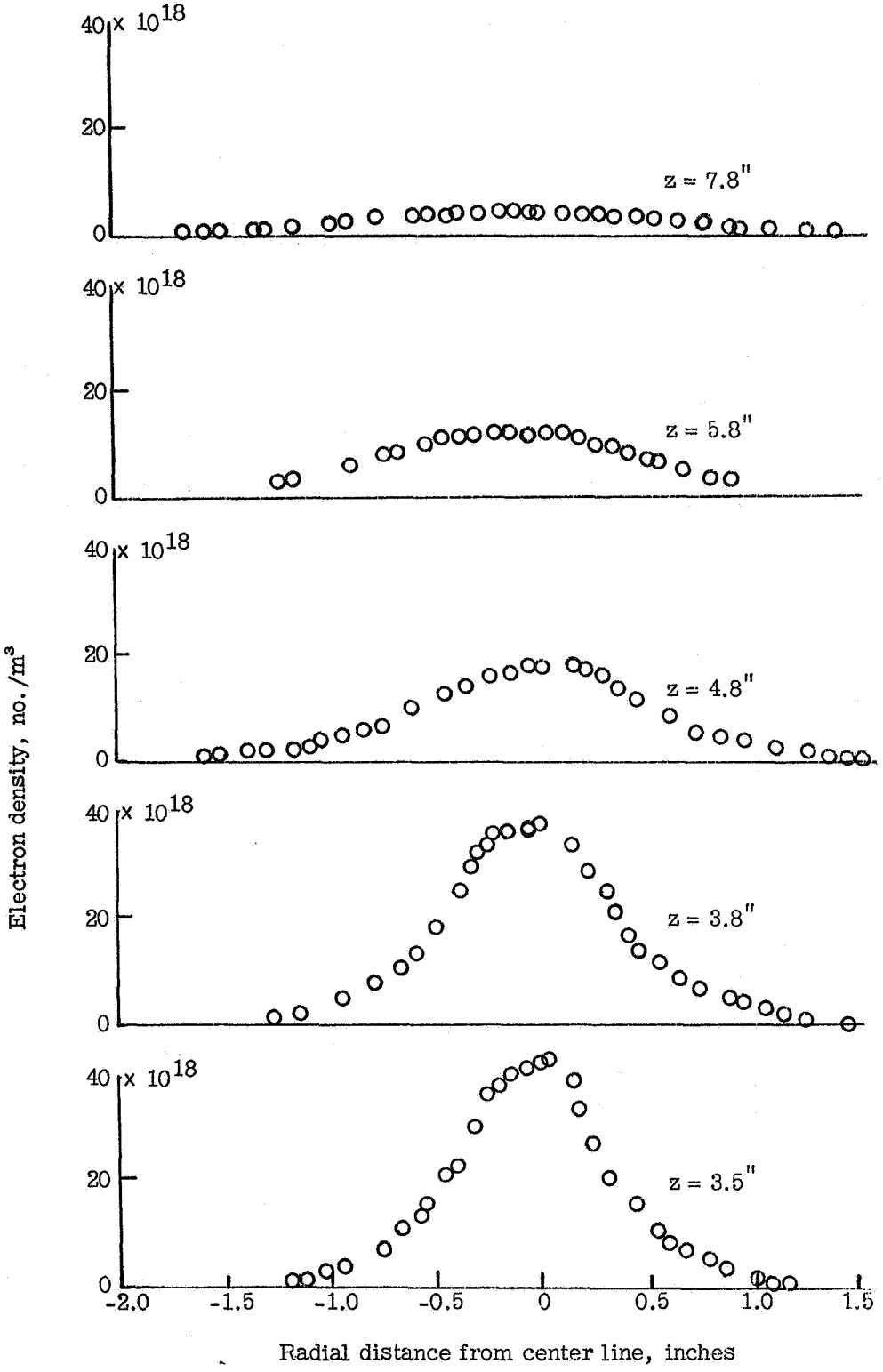

Figure 10.- Electron density as a function of r and z. I_{arc} = 100A, B = 700G.

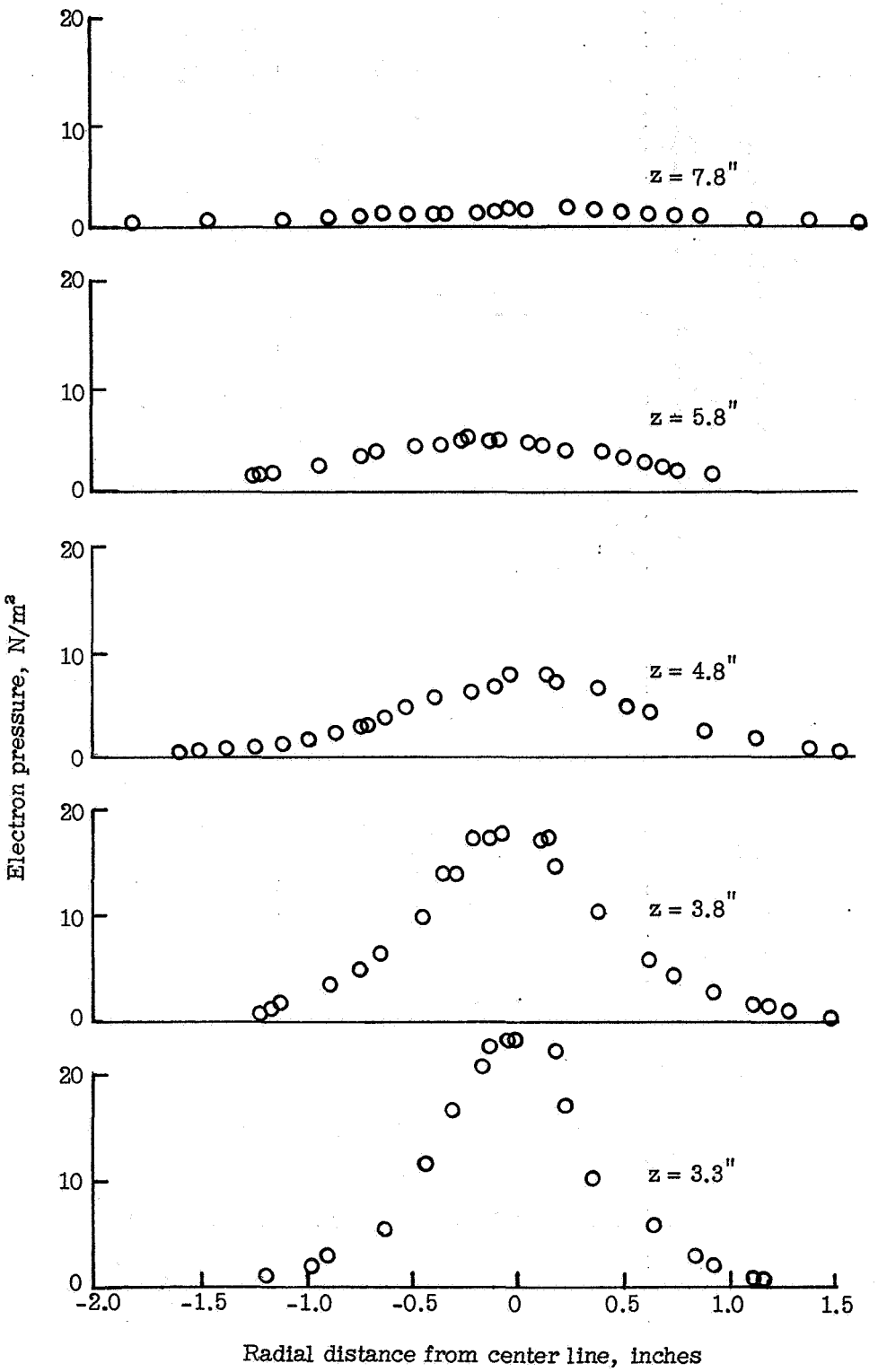

Figure 11.- Electron pressure as a function of r and z. I_{arc} = 100A, B = 700G.

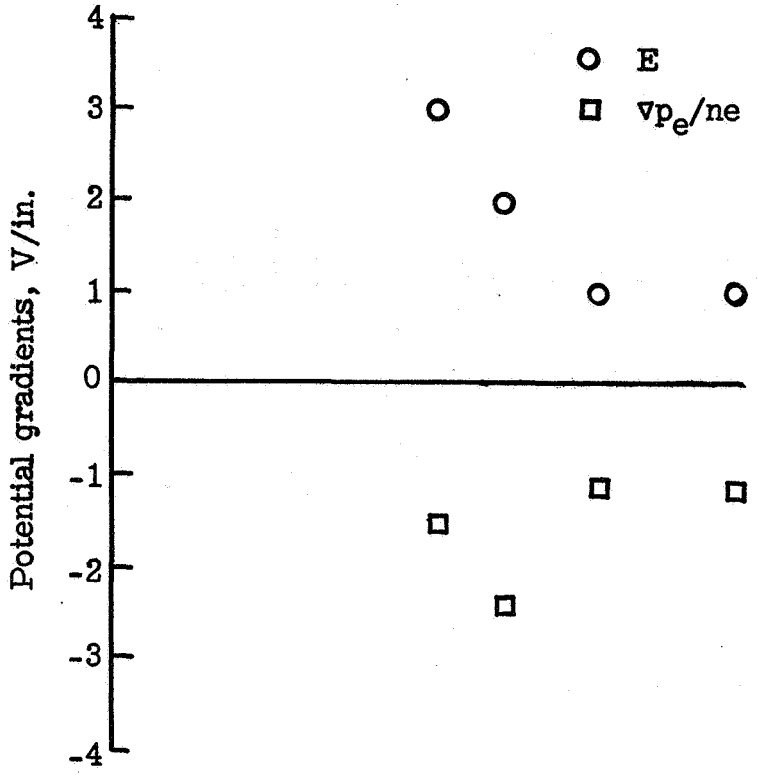

(a) r = 0

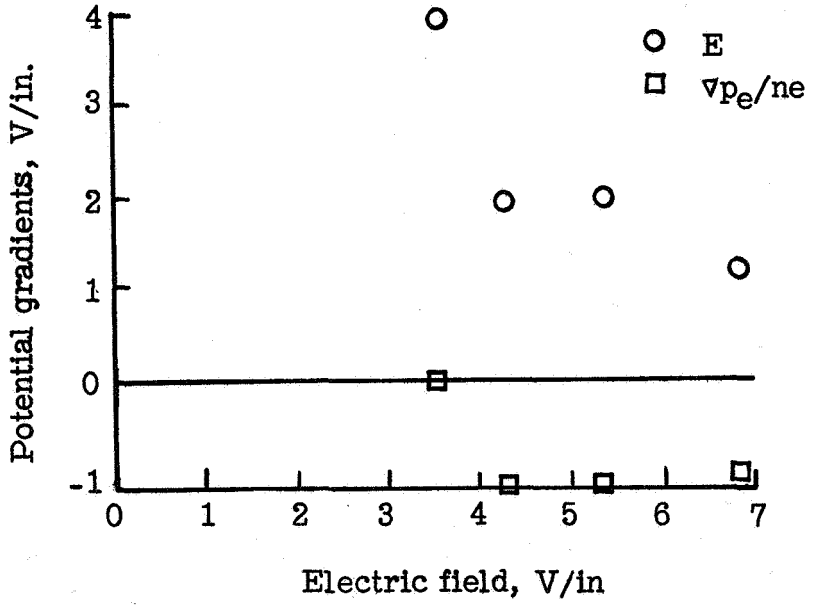

(b) r = 0.5

Figure 12.- Relative size of electric and electro-thermal fields.

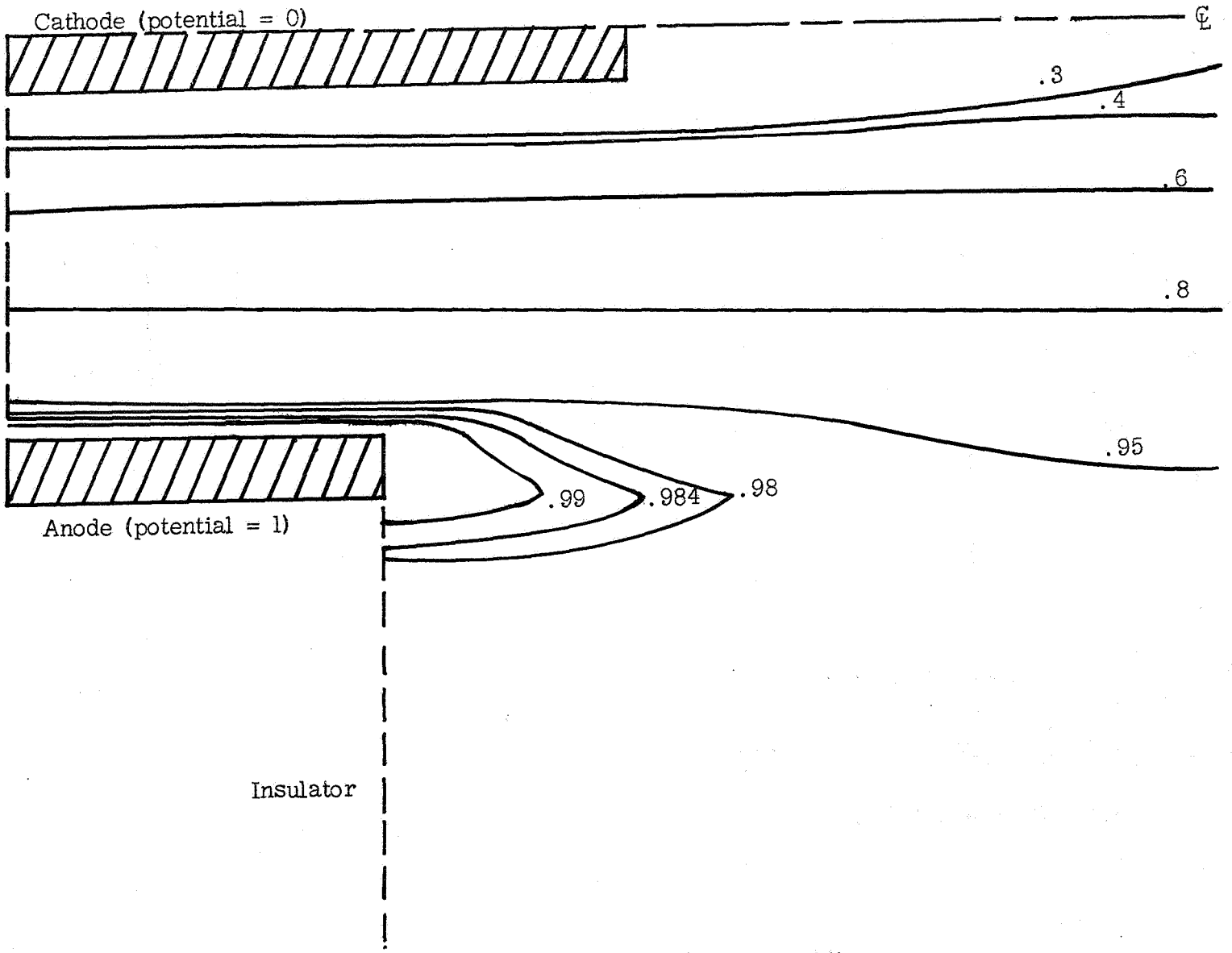

(a). Long cathode, high field (β = .01)

Figure 13.- Computed equipotentials.

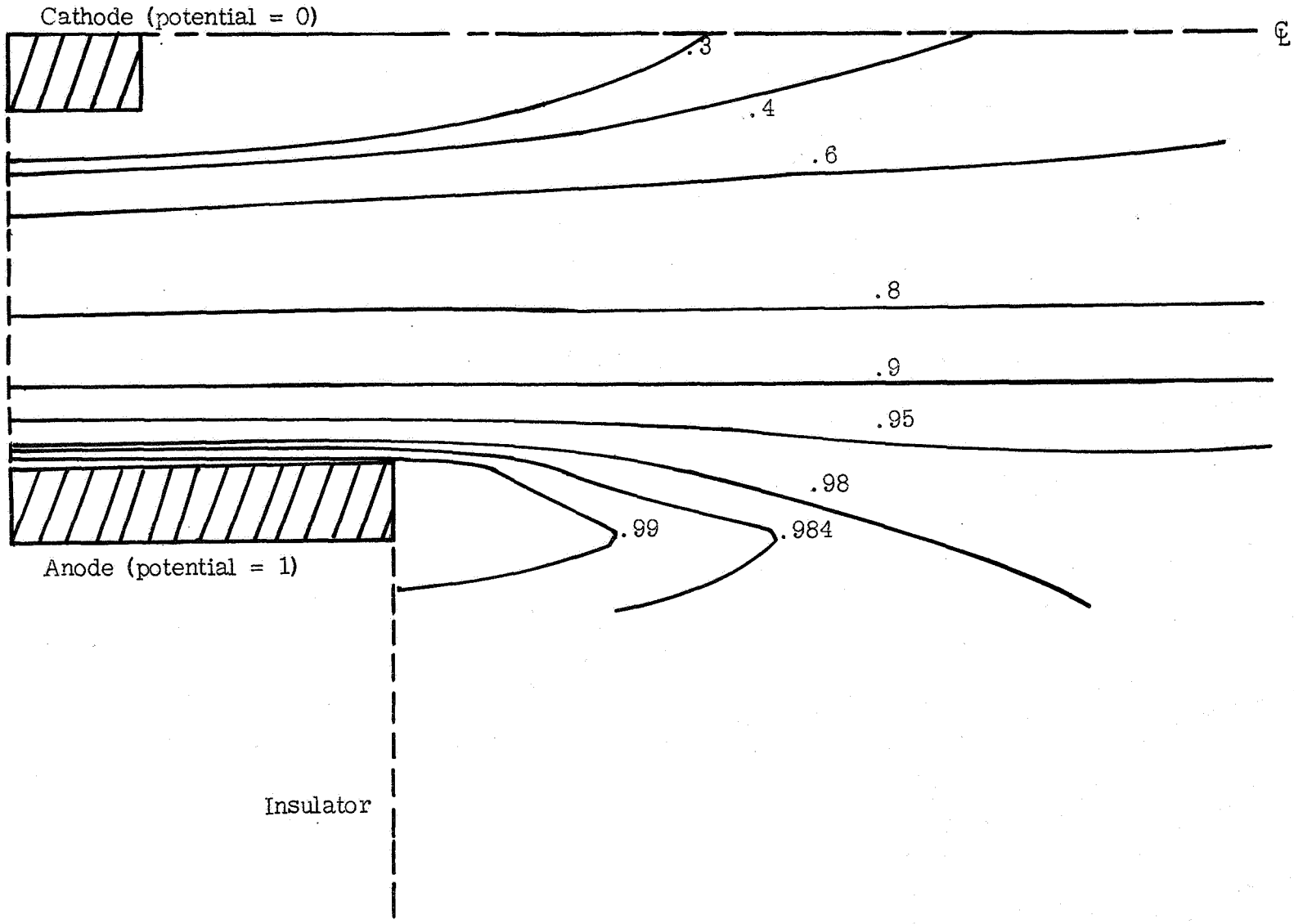

(b) Short cathode, high field (β = .01)

Figure 13.- Continued.

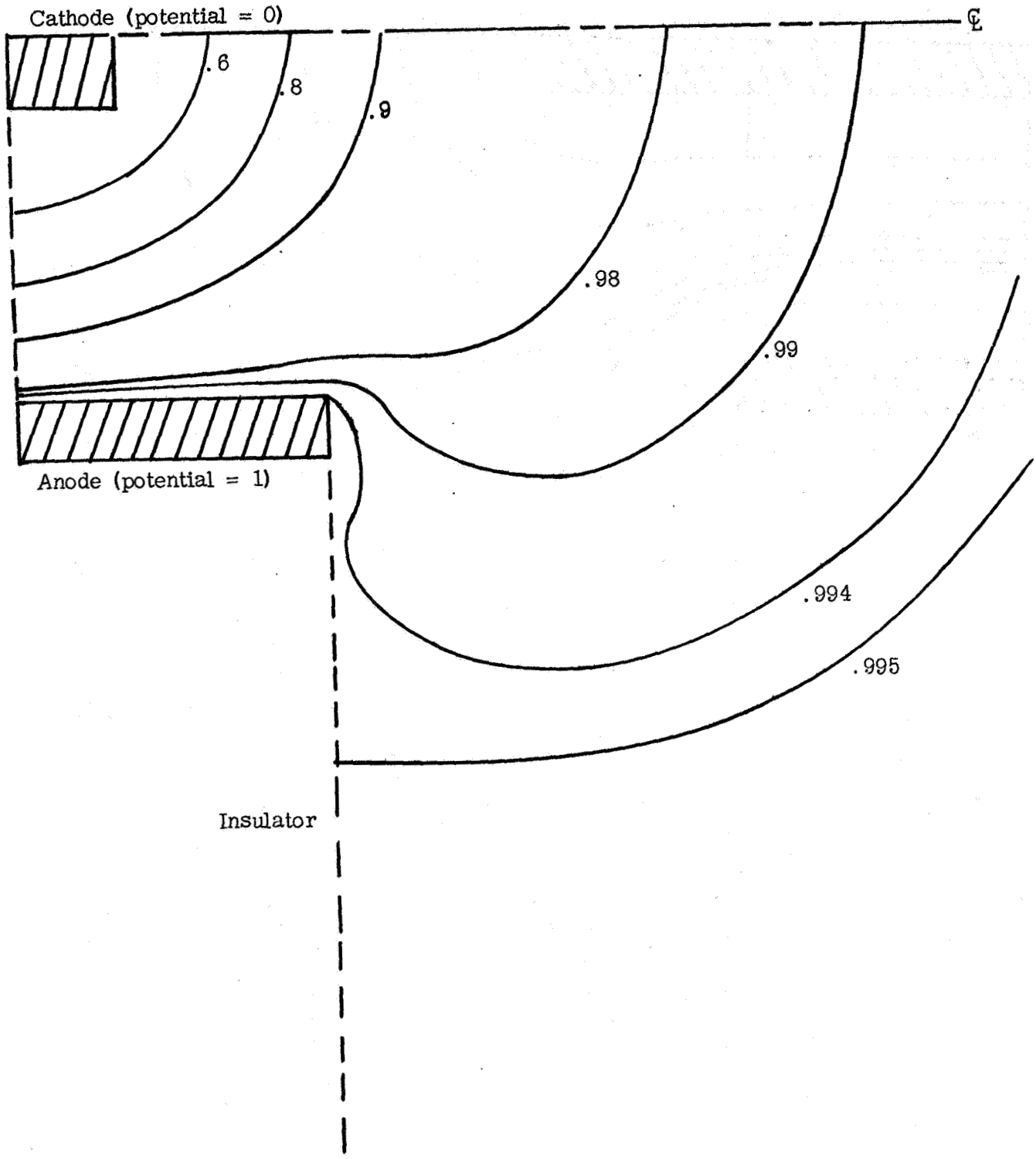

(c) Short cathode, zero field ($\beta = 1$)

Figure 13.- Continued.

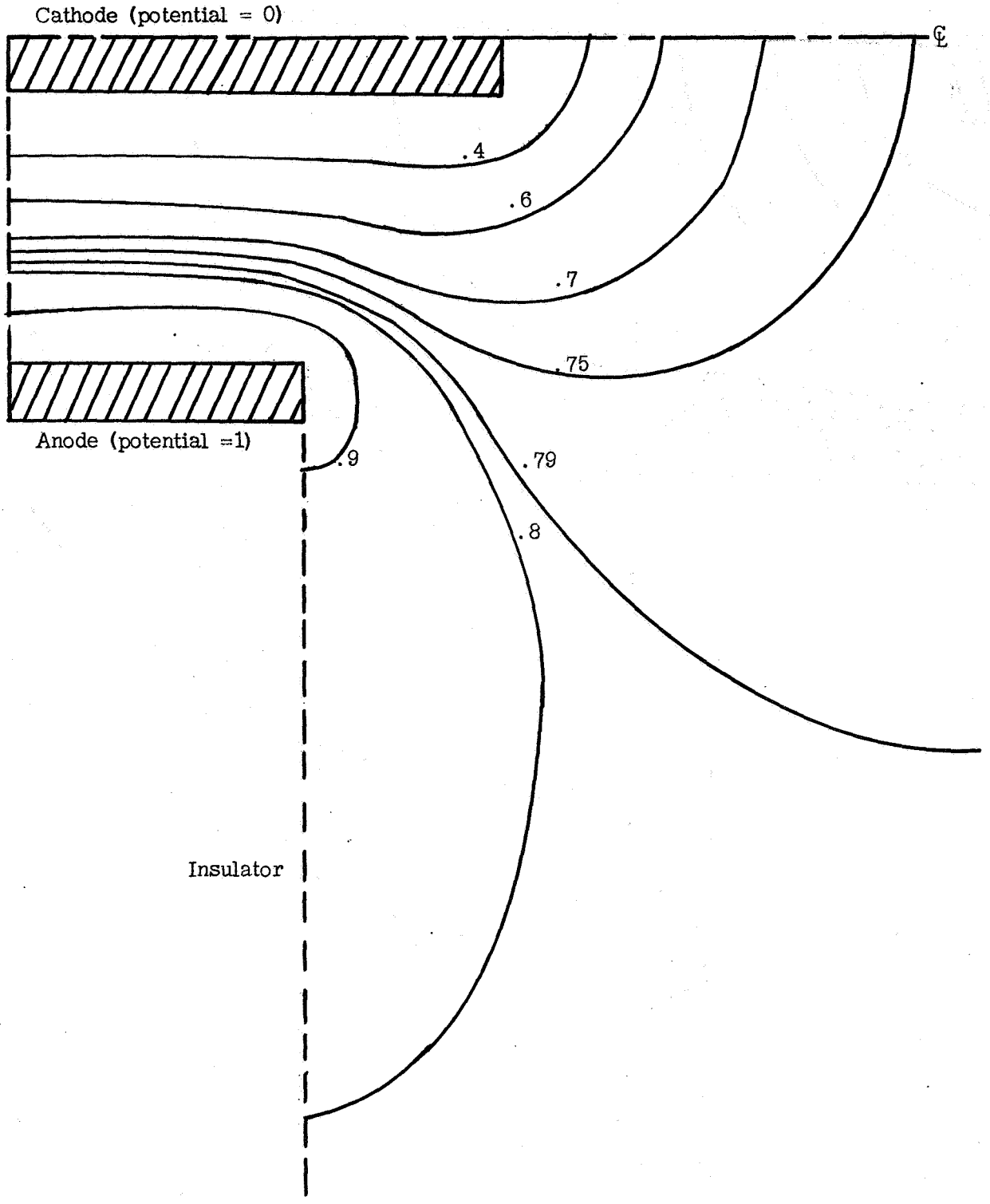

(d) Long cathode, zero field ($\beta = 1$)

Figure 13.- Concluded.

NASA-Langley, 1967